General Disclaimer

One or more of the Following Statements may affect this Document

- This document has been reproduced from the best copy furnished by the organizational source. It is being released in the interest of making available as much information as possible.

- This document may contain data, which exceeds the sheet parameters. It was furnished in this condition by the organizational source and is the best copy available.

- This document may contain tone-on-tone or color graphs, charts and/or pictures, which have been reproduced in black and white.

- This document is paginated as submitted by the original source.

- Portions of this document are not fully legible due to the historical nature of some of the material. However, it is the best reproduction available from the original submission.

Produced by the NASA Center for Aerospace Information (CASI)

STUDIES OF NEW MEDIA FOR RADIATION

INDUCED LASER

FINAL REPORT

JUNE 1984

K. S. Han, Y. J. Shiu, S. R. Raju, I. H. Hwang, B. Tabibi

National Aeronautics and Space Administration

Hampton Institute

Hampton, Va 23668

STUDIES OF NEW MEDIA FOR RADIATION

INDUCED LASER

FINAL REPORT

JUNE 1984

/

K. S. Han, Y. J. Shiu, S. R. Raju, I. H. Hwang, B. Tabibi

National Aeronautics and Space Administration

Hampton Institute

Hampton, Va 23668

FINAL REPORT

SUBMITTED TO:

National Aeronautics and
Space Administration
Langley Research Center
Hampton, Virginia 23665

INSTITUTION:

Department of Physics and
Engineering Studies
Hampton Institute
Hampton, Virginia 23668

TITLE OF GRANT:

Studies of New Media for
Radiation Induced Lasers

GRANT NUMBER:

NSG-1595

PERIOD COVERED BY THIS REPORT:

Feb 1, 1979 to April 30, 1984

PRINCIPAL INVESTIGATORS:

Kwang S. Han

RESEARCH ASSOCIATES:

Y.J. Shiu
S.R. Raju
I.H. Hwang
B. Tabibi

i

STUDIES OF NEW MEDIA FOR RADIATION INDUCED LASERS

K.S. Han
Y.J. Shieu*
S.R. Raju**
I.H. Hwang
B. Tabibi

Department of Physics and Engineering Studies

ABSTRACT

The purpose of this project is to investigate various lasants, especially, 2-iodohepafluoropropane (i-C_3F_7I) which could be used for the direct solar pumped lasers. During the period of Feb 1, 1979 through July 31, 1981. Y.J. Sheiu, research associate, achieved optical pumping of iodine laser using a small flashlamp. Using i-C_3F_7I as a laser gain medium, threshold inversion density, small signal gain, and laser performance at the elevated temperature were measured. The experimental results and analysis are presented in Chapter I.

During the period of Sept 1, 1981 through August 1, 1982, S.R. Raju, research associate made the numerical simulation of the iodine laser kinetics C_3F_7I and IBr system, using the model developed by J.W. Wilson. The results are presented in Chapter II and NASA Technical Paper 2182.

During the period of April 1, 1983 through April 30, 1984 I.H. Hwang, research associate, made the effort to evaluate the concept of a direct solar-pumped laser amplifier using (i-C_3F_7I) as the laser material, while another research associate Tabibi continued to make an effort of reevaluating several kinetic coefficient for i-C_3F_7I laser system. The results are discussed in Chapter III.

* present Address: Old Dominion University Department Norfolk, VA 23501

* "   "   University of Alabama Department of physics University, Alabama 35486

TABLE OF CONTENTS

Chapter I. IODINE LASER

1. INTRODUCTION

This chapter summarizes the experimental work done on the optical pumping
of an atomic iodoine laser using a small xenon flashlamp. Threshold inversion
density, small signal gain measurement and laser performance at elevated
temperature were studied.

High power laser beam offers the advantage of transmitting power without
the conventional power lines. This concept is especially useful in space
applications such as laser propulsion, space communication, space to space
power transmission and space to earth power transmission. Solar radiant
energy is the ideal energy source for these applications because the obvious
reason is no need to provide the energy source. A number of approaches to
convert solar energy into laser energy have been proposed.[1,2,3,] These systems
are electric discharge laser system (EDL)[4], Gas dynamics laser system (GDL)[5]
and optical pumped laser system (OPL)[3,6.] The EDL requires inefficient
conversion of solar energy into electric energy, although it is feasible
with present day's technology. The GDL requires heating the gas to high
temperature then expanding the gas rapidly to low temperature to achieve
the required population inversion. This involves heating, compressing and
cooling of the gas. Such a system is evaluated to be the heaviest solar
laser system requiring high launch cost, although its technology is well
established. Unlike EDL and GDL, the concept of a direct optically pumped
laser is rather simple. It means converting solar photons to laser photons
directly in a single energy conversion scheme.

Historically, there are numerous laser systems that were optically
pumped by flashlamps or lasers. Contrary to flashlamp output which is

1

intense and uv radiation on the short wavelength side of the 5700°K blackbody radiation. These will put constraints upon using solar photons as an optical pumping source. In the following, we summarized some of the important criteria for choosing an ideal lasant for space solar laser system:

1. Low threshold, because of the relative low intensity of solar radiation;

2. Broadband laser pumping mechanism and good overlapping between solar spectrum and the absorption spectrum of the lasant;

3. High quantum efficiency;

4. Reversible system for prolong period operation in space;

5. Operable at elevated temperature to minimize the radiator size.

2. IODINE LASER

In Wilson's paper[7], it was pointed out that a successful solar pumped laser is likely to be a photodissociation laser which lased from the atomic mestable state. A typical example of this class of laser is the alkyliodiode compounds that can be photolytically dissociated into the I^* $(P_{1/2})$ metastable state which then lases at 1.315 μm [8,9,10]. They have fairly large broadband absorption cross section centered at $\lambda=270$ mm with bandwidth of 200nm to 400nm depending on the different iodine compounds (Fig. 1). This rather broad pump band prompted the choice of atomic iodine laser as a candidate for solar pump band lasers although the absorption band lies at the near uv side of the solar spectrum. The kinetic pathway of this laser has been studied, and the energy level diagram is given in Fig. 2. Deactivation of the upper laser level can occur in a collision with an excited iodine atom and a parent molecule or any products of the photolysis. The iodine ground state $I(P_{3/2})$ will eventually be lost by recombing back into the parent molecule or by the formation of molecule iodine.

The rate of forming a stable alkyl dimer by two free radicals is very slow so that the chemical recycling requirement[11],[12] is modest for space application. The radiative life time of the upper state is 130 msec, and the life time is greater than 100 μsec. I_2 is the most important quencher of the laser, however I_2 is dissociated by the visible light of the solar spectrum and the effect of quenching is decreased. Because of the above reasons, the iodine laser has the potential of being a high gain and cw solar pumped laser.

The major disadvantage of the solar pumped iodine laser is the spectral mismatch between the laser pump band and the solar spectrum. For the absorption band of C_3F_7I from 250 nm to 300nm, there are about 1.2% of the total AMO solar radiation is usable. Other iodine compounds[13],[14] such as C_4F_9I and $(CF_3)_2 AsI$ shows a better spectral match, and 73% of the solar irradiance could be utilized for laser pumping. The small spectral efficiency, however, may be overcome by use of a large collection area and a high concentration of the solar radiation. Both are attainable with present space technology.

3. THRESHOLD INVERSION DENSITY

To determine the minimum solar concentration required for pumping an iodine laser, the threshold inversion density of the iodine laser system was measured. The threshold inversion density Δn can be determined from $r_1 r_2 T^2 G = 1$ where $G = \exp(2\sigma \Delta n \ell)$ at the threshold of laser emission, r_1 and r_2 are the mirror relectivities, T is the transmittance of the filter in the cavity, G is the small signal gain, σ is the stimulated emission cross section and ℓ is the cavity length (Fig. 3). The threshold condition was obtained by varying the value of T in this experiment. A linear xenon flashlamp was used as the pump source.

3

The power source for the flashlamp was $\geq$ 1.8 µF capacitor charged up to 7kV
The flashlamp was coupled to a quartz laser tube in an elliptical reflector
The flashlamp and the laser tube were located at focal points of the elliptics
so that the laser tube was illuminated isotropically. The laser tube had
Brewster angle windows and the cavity was formed with an aluminum-coated back
mirror that had 10 percent transmission at 1.32 µm. An InAs diode detector
was used for measuring the laser output power and a silicon detector was
used to minotor the flashlamp light output.

The absolute intensity of the xenon flashlamp was obtained by comparing it
against a standard carbon arc. A 0.5-m McPherson spectrometer was used to
record the spectra of both sources on Kodak 101-01 film.

Fig. 4 shows the spectra of the carbon arc and the xenon flashlamp in
the range from 250 to 360 nm. The mercury lines were used for wavelength
indication. Conversion of the film density into intensity showed that the
peak intensity of the flashlamp spectrum was located near 300 nm which
corresponds to a blackbody temperature of 9600°K. The total source intensity
in the pumpband from 250 to 290 nm is then obtained by:

$$I \, \Delta\lambda = \int_{250}^{290nm} I(\lambda)d\lambda$$

$$= 3.75 \times 10^2 \text{ W cm}^{-2} \text{ sr}^{-1}$$

The xenon flashlamp had a diameter of 0.5 cm and a length of 10 cm. Therefore
the total UV power is 2.36×10^4 W. Since the flashlamp pulse duration was
12 µs, the radiant energy E_{uv} in the UV band is 0.28J. This value can be used
to estimate the inversion density Δn produced by the flashlamp. Since $(I) \ll (I^*)$:

$$\Delta n = (I^*) = \frac{E_{uv}}{\langle h\nu \rangle (vol)}$$

4

where (I) and (I^*) are the concentrations of the ground state and the excited state iodine atoms in the laser system, respectively. The average photon energy $\langle h\nu \rangle = 4.5$ eV and (vol) is the volume of the laser tube ($\sim$120 cm^3). η is the overall efficiency of pumping the iodide and can be expressed as:

$$\eta = \eta_r \cdot \eta_t \cdot \eta_g \cdot \eta_\alpha$$

where η_r is the reflectivity of the reflector (60 percent for aluminum), η_t is the transmittance of the quartz tube wall ($\sim$90 percent), and η_g is the geometrical efficiency of the reflector used ($\sim$90 percent), and η_α is the absorption coefficient of the lasant ($\sim$45 percent for C_3F_7I). Hence:

$$\eta = 0.22$$

Insertion of these values into the above equation yields the inversion desnsity:

$$\Delta n = 7 \times 10^{14} cm^{-3}$$

The iodine laser system reached the threshold condition ($r_1 r_2 T^2 G$:) with T = 92 percent (the transmittance of the filter in the cavity), r_1 = 96 percent, and r_2 = 90 percent. The gain G of the system therefore was 1.37 or a round trip gain of 2.3 percent per cm. From the relation G = exp $(2\sigma(\Delta n)\ell)$ and $\sigma = 6 \times 10^{-18}$ cm^{-2} the stimulated emission cross section for 20 Torr C_3F_7I, we obtain $\Delta n = 9 \times 10^{14} cm^{-3}$ which is in general agreement with the value $7 \times 10^{14} cm^{-3}$ obtained from the pumping energy. Since the threshold condition above neglects the transmittance of the two Brewster windows, the gain and the threshold inversion density are actually somewhat lower. If 98 percent transmission is assumed for the windows, the overall transmission $T' = (.98)(.98)(.98) = .882$ which results in a 32.6 percent loss cavity with G = 1.48 and $\Delta n = 1.1 \times 10^{-5} cm^{-3}$.

The minimum cavity loss is limited by the absorption of the Brewster windows ($\sim$7.8 percent) and the mirror loss of 2 percent may be a practical choice.

The overall cavity loss then become ~10 percent. For such a low loss cavity:

$$\Delta n_{(min)} = 3.4 \times 10^{14} cm^{-3}$$

The minimum UV energy density U required for the inversion is:

$$U = \Delta n \, h\nu = (3.4 \times 10^{14} cm^{-3}) (4.5 eV)$$
$$= 18.36 \times 10^{-5} Jcm^{-3}$$

This value corresponds to the energy of the UV band of 11 solar constants for one second. Since solar concentrations of over 1,000 are common practice requirement for the threshold energy seems easily satisfied by a solar concentrator in space.

4. GAIN MEASUREMENT

To determine optimum operating conditions of solar pumped iodine laser the small signal gain measurement was performed. The experimental set up included an oscillator and an amplifier, both were pumped by xenon flashlamps. The oscillator signal was sent through the amplifier, signals were measured by two InAs detectors D_M and D_A, where D_M is the monitor signal and D_A is the amplifier signal (Fig. 5.) Ratio of $(D_A/D_M)o$ was obtained without pumping the amplifier, and then $(D_A/D_M)p$ was obtained with flashlamp pumping the amplifier. The amplifier tube was filled with the same gas when we took both ratios. G is the small signal gain and G is defined as

$$G = \frac{\left(D_A/D_M\right)_p}{\left(D_A/D_M\right)_o}$$

G can also be obtained by $G = exp(\Delta n.\sigma.\ell.)$ from theory, where Δn is the inversion density, σ is the stimulated emission cross section and ℓ is the gain length.

Fig. 6 gave typical results of small signal gain measurement. A linear increase of small signal gain with pumping energy was observed (Fig. 7), this was expected since increasing energy produced more atomic iodine in the excited state. At constant pumping power, the excited state produced was proportional to the gas pressure while the stimulated cross section decreased as pressure went up. Therefore it

6

showed a maximum in the profile (Fig. 8). The optimum pressure for lasing was from 10 Torr to 20 Torr. The time variation of the small signal gain indicated that energy storage time for the upper laser level was 1 msec order (Fig. 9).

5. LASER PERFORMANCE AT ELEVATED TEMPERATURE

In this study, a laser was put inside a cylindrical oven of 2" i.d. with a xenon flashlamp parallel to the laser tube. The seals of the flashlamp was cooled by blowing air. Oven temperature was measured by thermo couple. Laser cavity was formed by two laser mirrors outside the oven. In front of each mirror, there was an iris whose opening was minimized (typically $\lesssim 3mm$) to insure single mode oscillation. Laser signal was detected by an InAs detector. The flashlamp output was monitored by a silicon detector. Through the whole temperature range, the variation of the signal from silicon detector was no greater than 10%. The iodine bearing compound used was C_3F_7I. The gas introuced into the laser tube with typical waiting time of 5 min. before flashlamp was fired.

Variation of the peak laser output with temperature at fixed gas number density was given in Fig. 10. C_3F_7I pressure at 300 $^\circ$K was 5 Torr. We observed a gradually decreasing of the laser output with increasing temperature. Lasing stopped at 660 $^\circ$K, at this temperature, gas pressure of up to 50 Torr was used with no lasing observed. Peak laser output at T = 600 $^\circ$K was 50% of its value at T = 300 $^\circ$K. Fig. 11 gave the variation of the total pulse length with temperature and the time delay of the first laser pulse with respect to the firing of the flashlamp pulse. Laser pulse occurred about the same time until $\lesssim$ 600 $^\circ$K. The pulse length was decreased by 50% at T = 600 $^\circ$K.

For a fixed number density gas in a laser tube, there are at least three factors affecting the laser performance when temperature is changing:

(1) reaction rates are temperature dependent
(2) pyrolysis of the parent gas
(3) temperature dependence of the Einstein coefficient of the stimulated interaction.

The temperature dependence of stimulated transition is given by

$$A_{21} = \frac{c^3 f(\nu)}{4\pi^2 \nu^2 t_{sp}} \Delta\nu$$

which also depends on the Doppler broadening of the laser transition.

Because of lack of data on (2) and (3), we were not able to analyze these two factors with Doppler broadening. However, experimental results indicated that photodissociation iodine laser was capable of operation at temperature up to 600 °K with only 50% decrease of its peak power output.

6. PARAMETER STUDY OF IODINE LASER PUMPED BY 5KW TAMARACK SOLAR SIMULATOR

In this study, a kinetic model developed by Wilson[12] was used for parameter study. The kinetic equations and rate coefficients from Wilson and Lee [12] was listed in Tables 1 and 2. The tamarack solar simulator has 5 KW output in beam, the irradiance survey of the solar simulator output gave an average of 14,700 solar concentration over 5.6 cm long when a cone shaped collector was used to concentrate the output beam. Other important information included cavity length = 56 cm, radius of laser mirrors = 10 m, reflectivity of laser mirror = 99.5%, and output mirror transmission was 3% typically. Fig. 12 and 13 gave computer laser outputs corresponding to 3 msec and 15 msec solar simulator pulse respectively. Fig. 14 to Fig. 17 summarized the parameter study under various conditions. I_2 and O_2 were the most important quencher of the upper laser level, and the effect of I_2 and O_2 impurities were given in Fig. 18 and Fig. 19. Fig. 20 gave the laser pulses when successive solar simulator pulses were pumping the same gase filling. The details are found in Ref 25 and NASA Technical paper 2182 (1984).

8

REFERENCES

1. J. Rather, E. Gerry and G. Zeiders, "Investigation of Possibility for solar Powered High Energy Lasers in Space," W.J. Schafer Assoc., Inc., Report 77SR-VA-U3, May 25, 1977.

2. W. S. Jones, "Space Laser Power Systems," American Institute of Aeronautics and Astronautics, Inc.m 79-1013, 1979.

3. R. T. Taussing, C. Bruzzone, L. Nelson, and D. Quimby W. Christiansen, "Solar-Pumped Lasers for Space Power Transmission," American Institute of Aeronautics and Astronautics, Inc., 79-1015, 1979.

4. P. K. Baily and R. C. Smith, "Closed-Cycle Electric Discharge Laser Design Investigation," Final Report, Hughes Aircraft Co., prepared for the NASA-Lewis Research Center, March 1978.

5. W. E. Young and G. E. Kelch, "Closed-Cycle Gas Dynamics Laser Design Investigation," NASA Report CR-135130, prepared by the Pratt and Whitney Aircraft Group, United Technologies Cooperation, January 1977.

6. O. Yesil and W. H. Christiansen, J. Energy, 3,49, 1979.

7. J. W. Wilson, "Solar Pumped Gas Laser Development," NASA TM-81894, December 1980.

8. J. V. V. Kasper, J. H. Parker and G. C. Pimental, J. Chem. Phys., $\underline{43}$, 1827, 1965.

9. J. V. V. Kasper and G. C. Pimental, Appl. Phys. Letter 5, 231 (1964).

10. R. W. F. Gross and J. F. Bott, Handbook of Chemical Lasers, edited by John Wiley and Sons, Chap. 12 (1976).

11. G. A. Fisk, Sandia Lab., SAND 77-0880 (1977).

12. J. W. Wilson and J.H. Lee, Virginia J. of Science, $\underline{31}$,34 (1980).

13. G. N. Birich, G. I. Drozd, V. N. Sorokin and I. I. Struk, JETP Lett, 19, 240 (1974)

14. Andrewa, G. N. Birich, V. N. Sorokin and I. I. Struk, Sov. J. Q.E., $\underline{6}$ 781 (1976).

15. J. H. Lee and W. Weaver, to be published.

16. C. R. Giuliano and L. D. Hess, J. of App. Phys. $\underline{38}$, 4451 (1967)

17. B. F. Gordiets, L. I. Gudzenko and V. Ya Panchenko, JETP Lett. $\underline{26}$, 152 (1977).

18. Yu B. Konev, N. I. Lipatov, P. P. Pashinin and A. M. Prokhorov, Sov. Tech. Phys. Lett. 5 (4), 1979.

19. R. E. Beverly and M. C. Wong, Optics Communication, 20, 23 (1977).

20. C. E. Turner, N. L. Rapagnani, N76-75267 (1972).

21. K. Hohla and K. L. Kompa, J. Naturforseh, $\underline{27a}$, 938 (1972).

22. J. A. Blake and George Burns. J. of Chem. Phys., _54_, 1480 (1971).

23. K. H. Stephan and F. J. Comes, Chem. Phys. Lett. _65_, 251 (1979).

24. D. H. Burde and M. A. McFarlane, J. of Chem. Phys., _64_, 1850 (1976).

25. J. H. Lee, Y. J. Sheiu and W. R. Willard Southeast con. 1980, IEEE, P 126-131

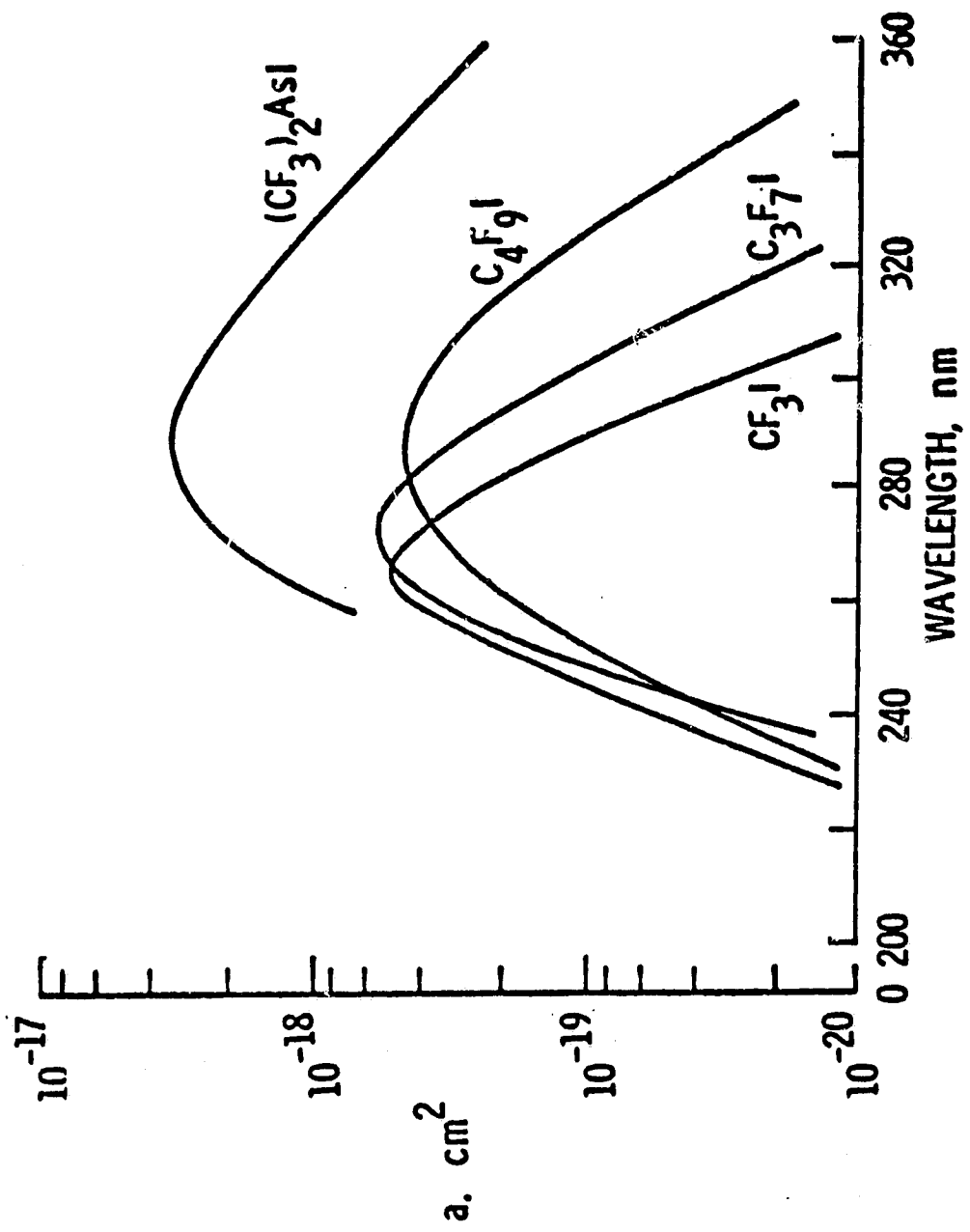# ABSORPTION CROSS SECTIONS OF PERFLUOROALKYL IODIDES

Fig. 1

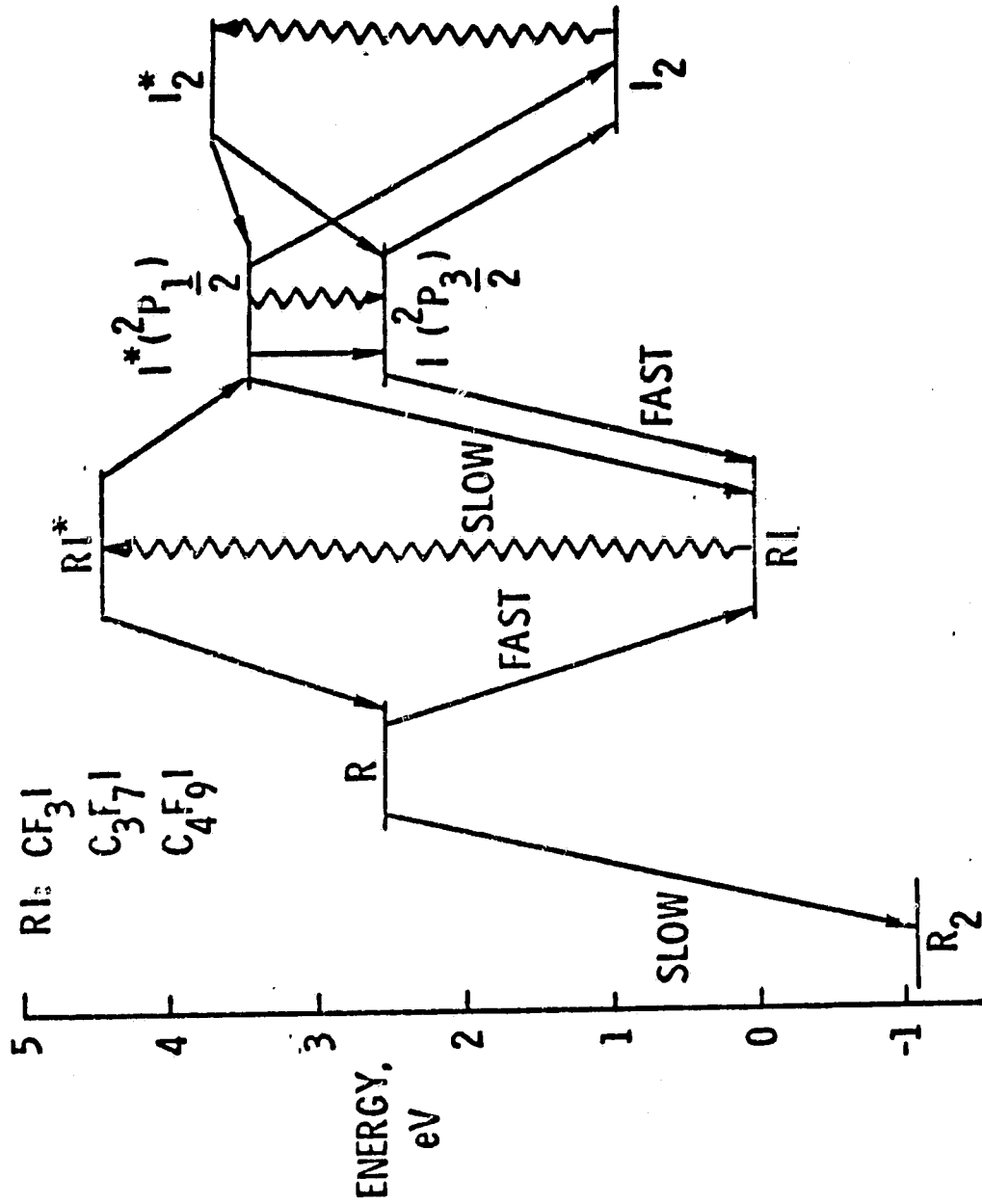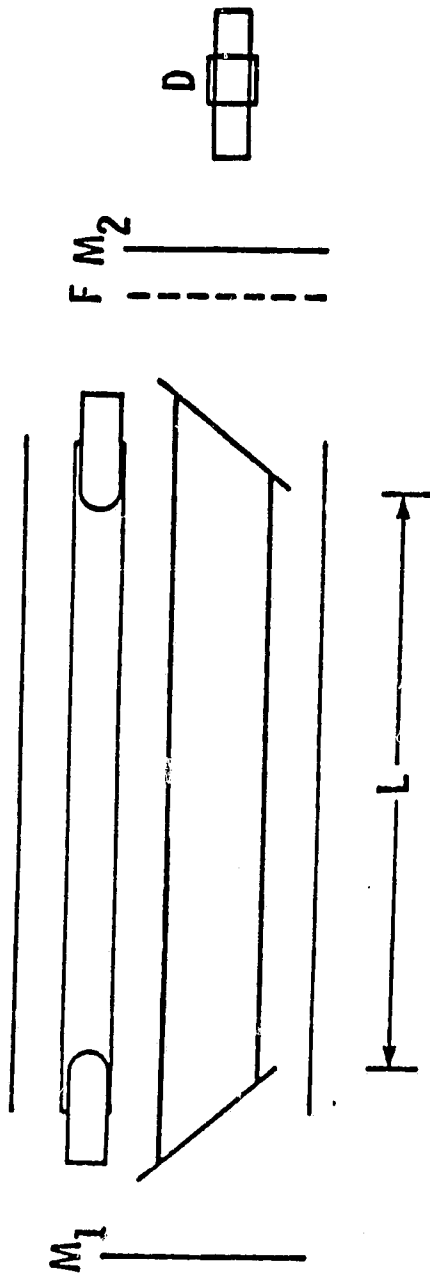11

SOLAR PUMPED ATOMIC IODINE LASER DIAGRAM

Fig. 2

IODINE LASER THRESHOLD MEASUREMENT

$G = EXP\ (2\sigma\Delta nL)$

σ: STIMULATED EMISSION COEFFICIENT
Δn: INVERSION POPULATION DENSITY
L: PUMPING LENGTH

$r_1 r_2^2 T^2 G = 1$ AT THRESHOLD

r_1, r_2: MIRROR REFLECTIVITY
T: FILTER TRANSMISSION

Fig. 3

SPECTRA OF THE XENON FLASHLAMP
AND A STANDARD CARBON ARC

FILM DENSITY
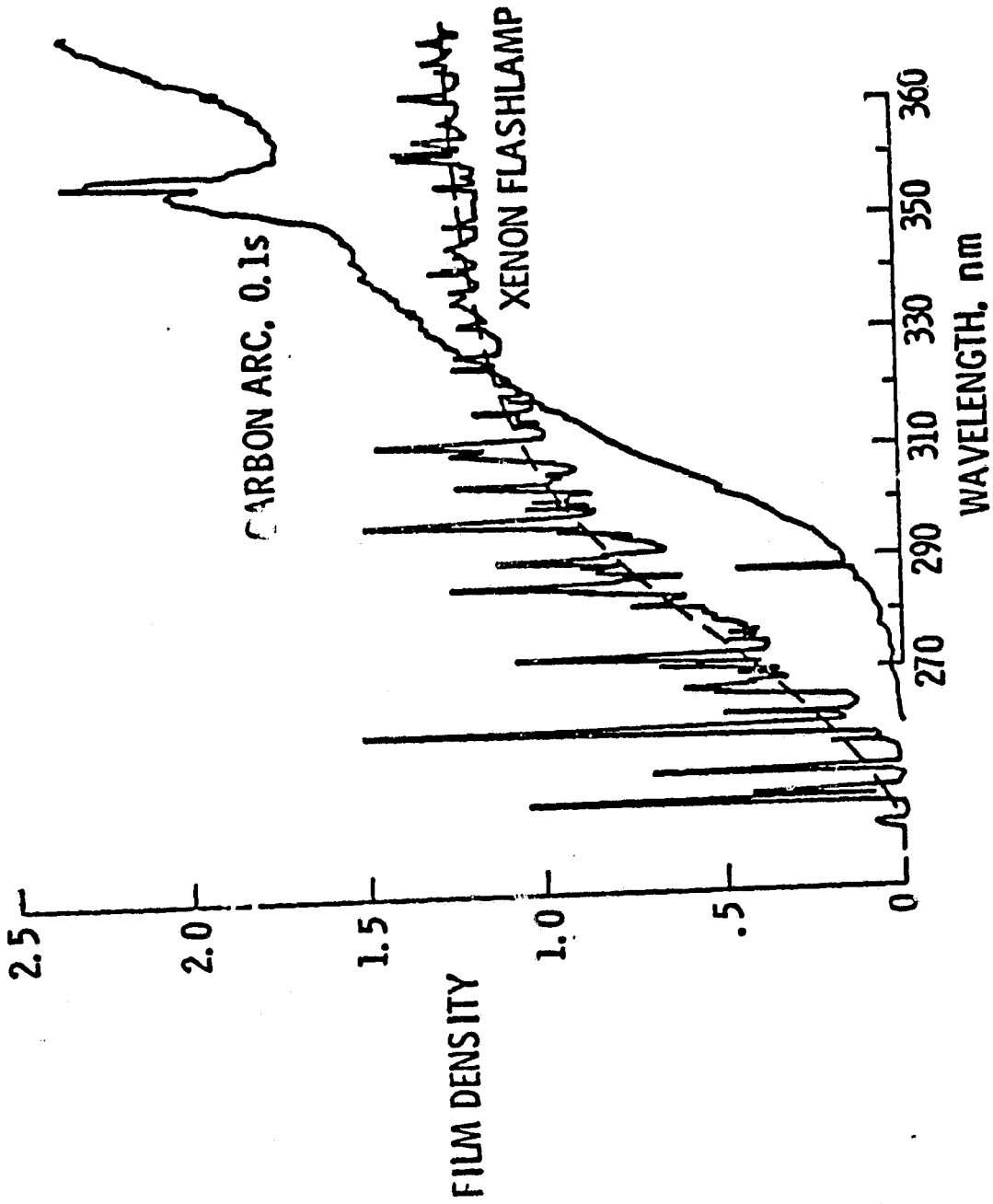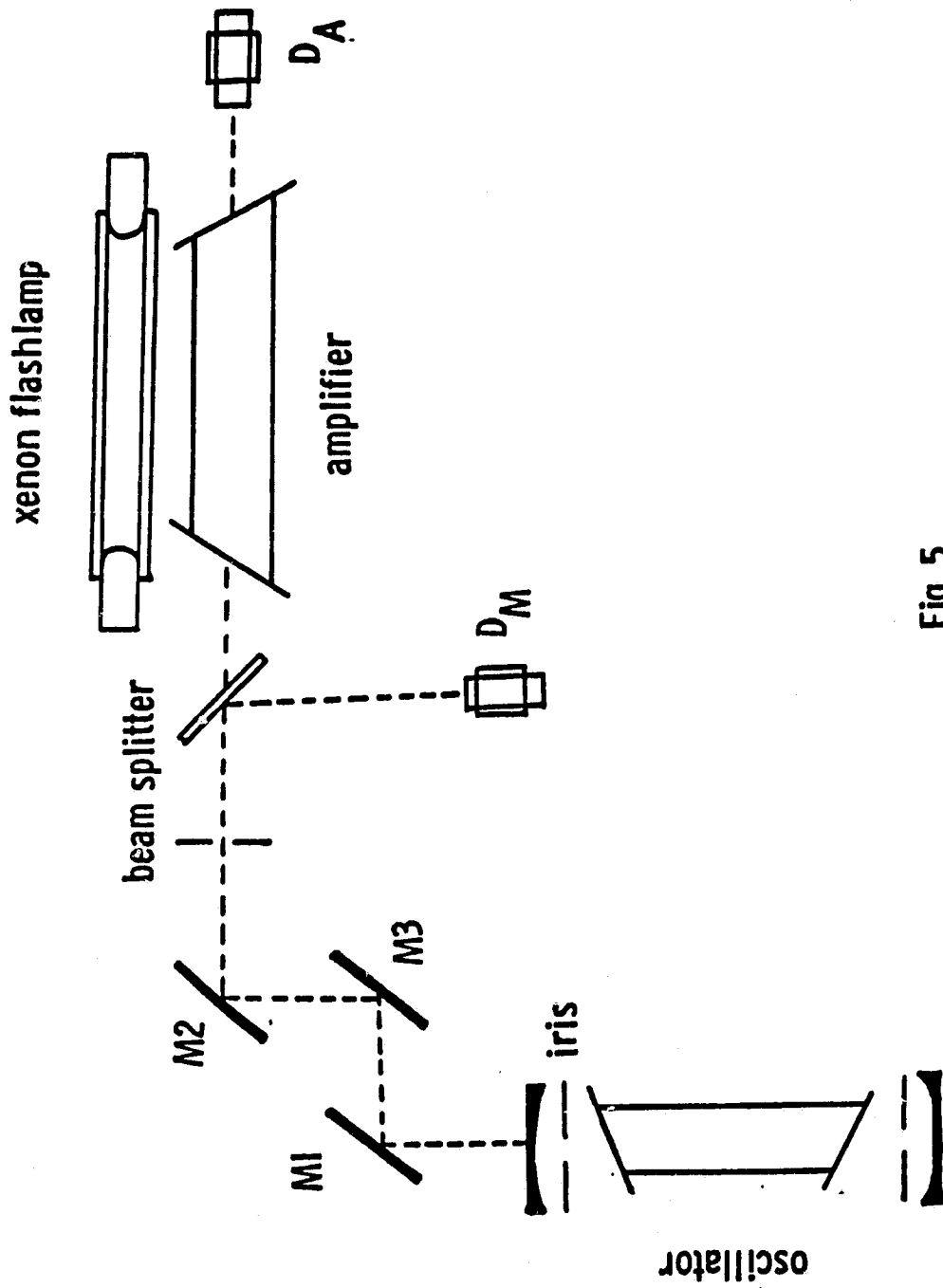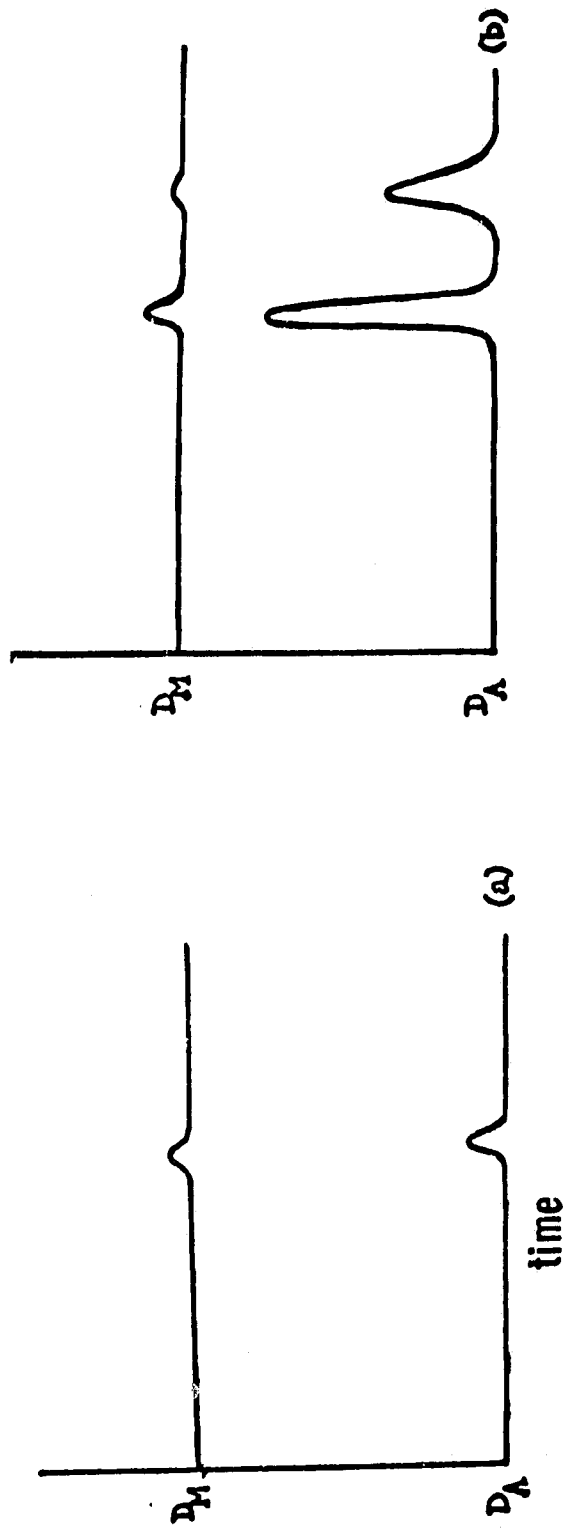
CARBON ARC. 0.1s

XENON FLASHLAMP

WAVELENGTH, nm

Fig. 4

EXPERIMENTAL ARRANGEMENT FOR GAIN MEASUREMENT

Fig. 5

Typical signals obtained without(a) and with(a) flashlamp pumping the amplifier
oscillator output delayed 1.2 msec w.r.t. amplifier pumping pulse
(scale: 5mv/cm : 2μsec/cm)

Fig. 6

16

SMALL SIGNAL GAIN vs. PUMPING ENERGY OF THE AMPLIFIER
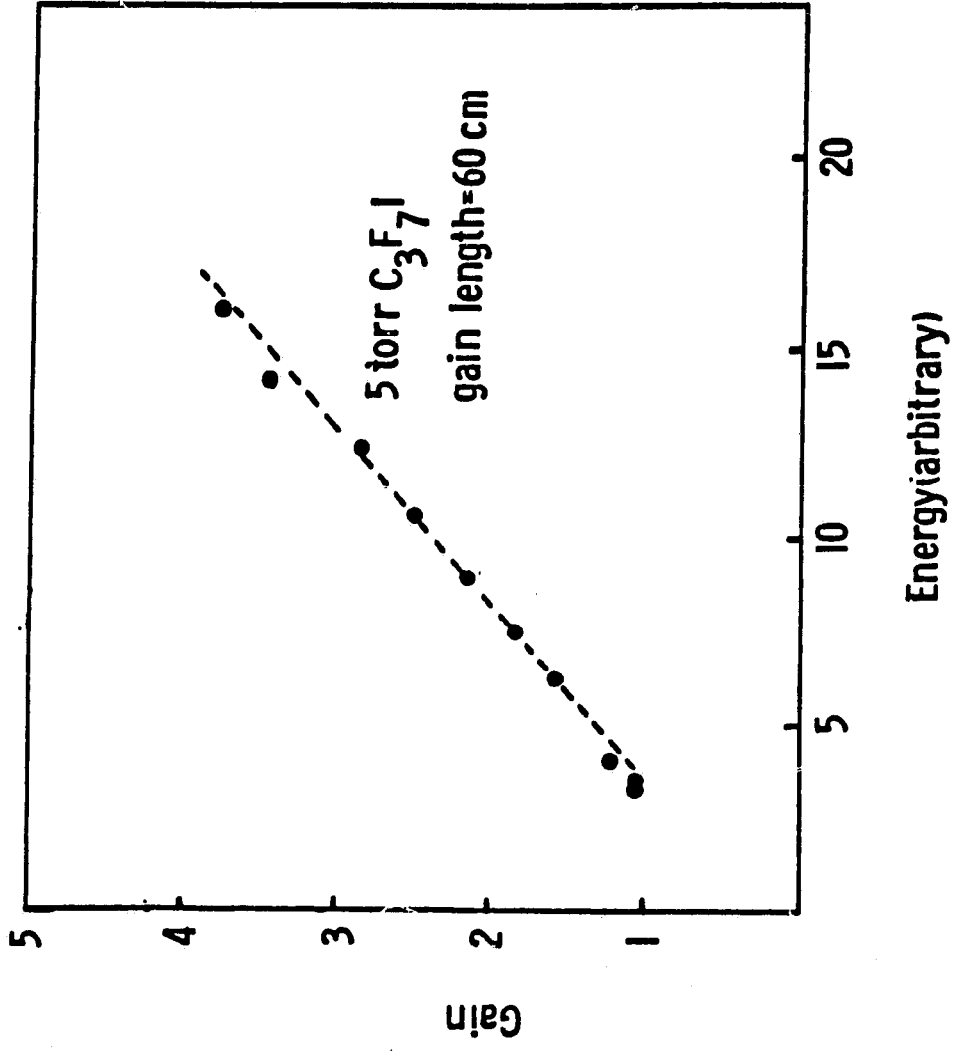

5 torr C_3F_7I
gain length=60 cm

Gain

Energy(arbitrary)

Fig. 7

SMALL SIGNAL GAIN vs. GAS PRESSURE

Xe flashlamp 1.8 KV
oscillator output delayed 0.8 msec
w.r.t amplifier pumping pulse

Gain

Pressure (torr)

Fig. 8

SMALL SIGNAL GAIN vs. TIME

xe flashlamp
4 KV(3200 J)

time(msec)

10 torr C_3F_7I

gain length =60 cm
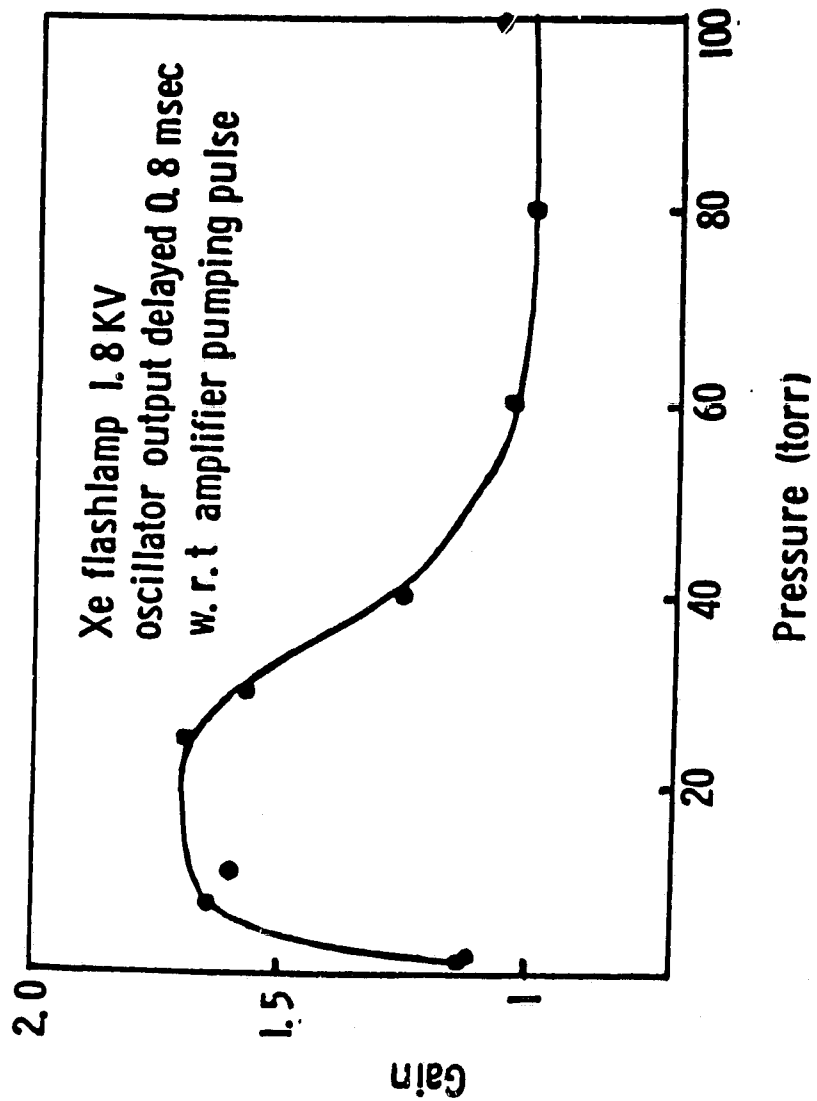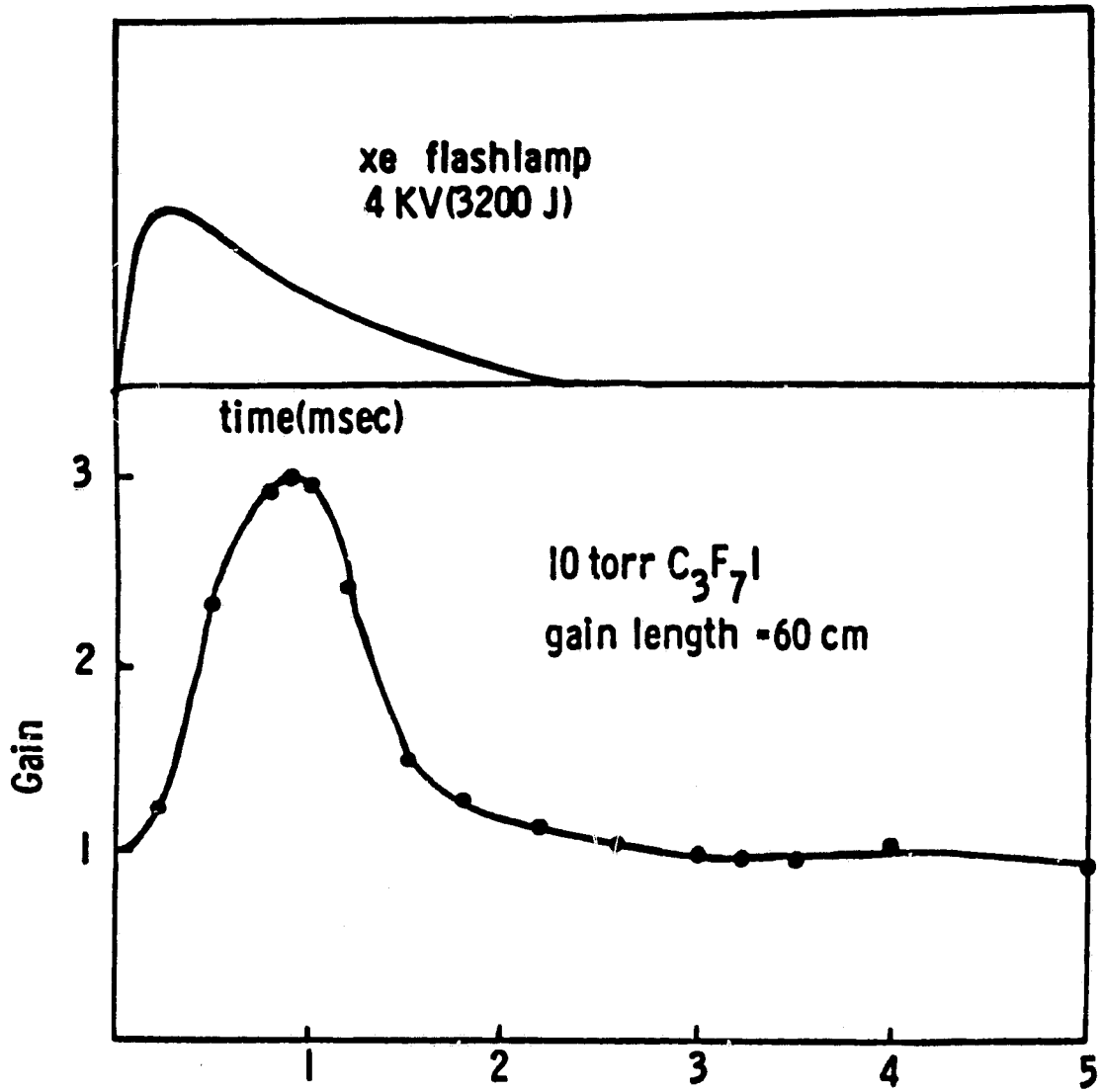
Gain

time delay of the oscillator output w. r. t. the amplifier
pumping pulse

Fig. 9

LASER OUTPUT vs. TEMPERATURE AT FIXED NUMBER DENSITY

15 torr C_3F_7I at 300 K

temperature(K)

laser output (arb. unit))
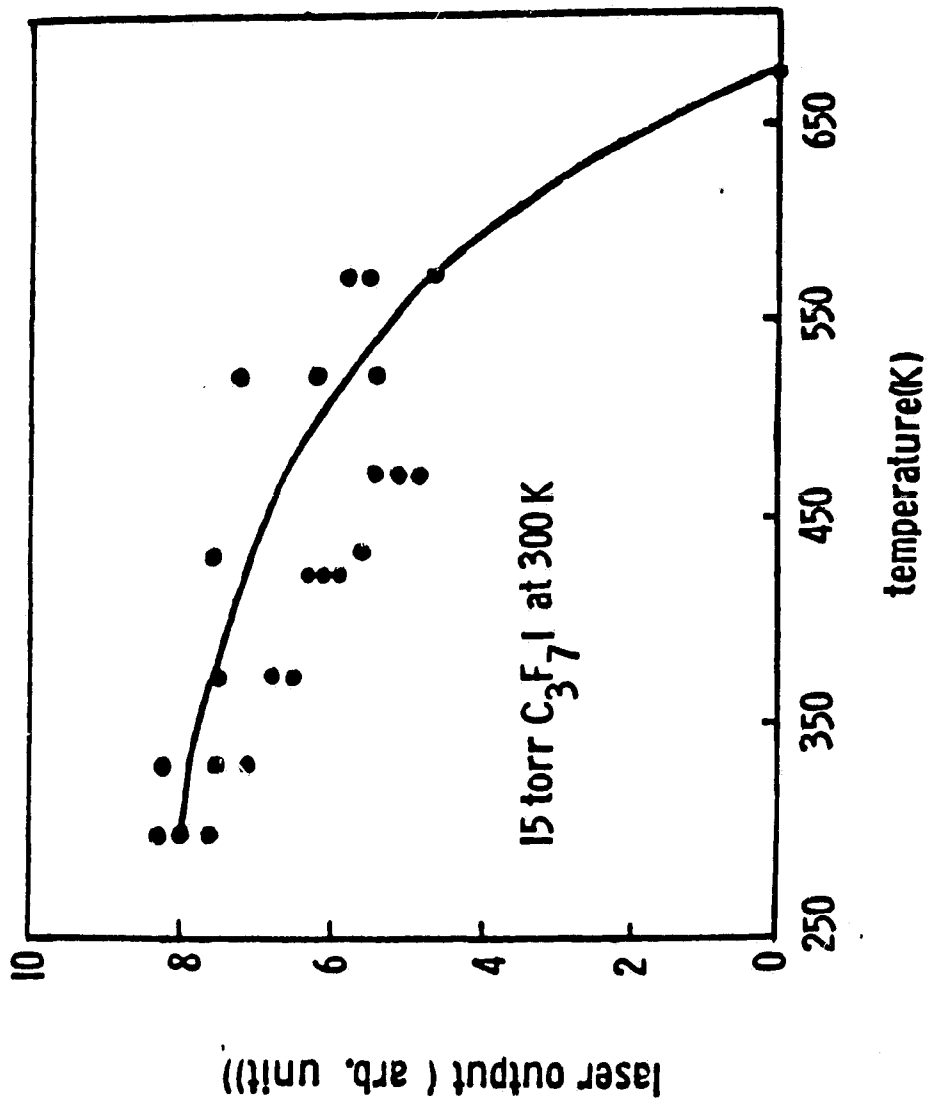
Fig. 10

20.

LASER PULSE LENGTH vs. TEMPERATURE
AT FIXED NUMBER DENSITY
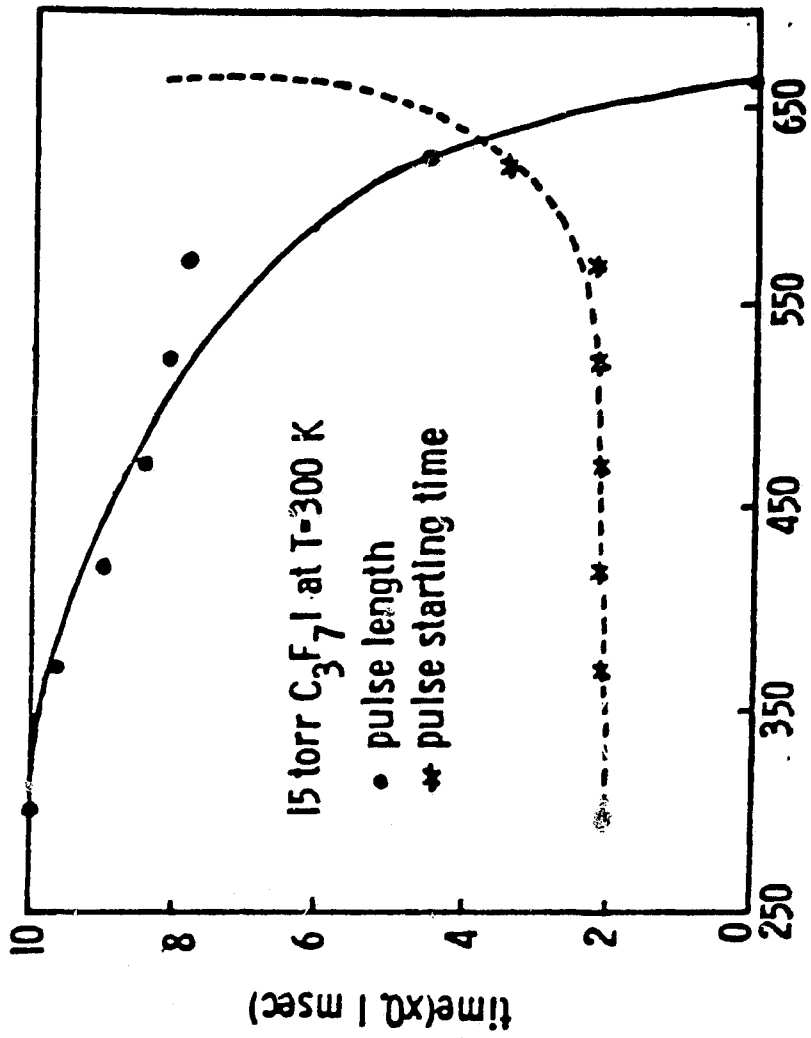
15 torr C_3F_7I at T=300 K
● pulse length
✳ pulse starting time

temperature(K)

Fig. 1i

time(x0.1 msec)

10   8   6   4   2   0

250   350   450   550   650

Fig. 12 IODINE LASER OUTPUT

22

Fig. 13   IODINE LASER OUTPUT

solar simulator pulse

p=10 Torr

p=25 Torr

laser output(watts)

time(msec)

23
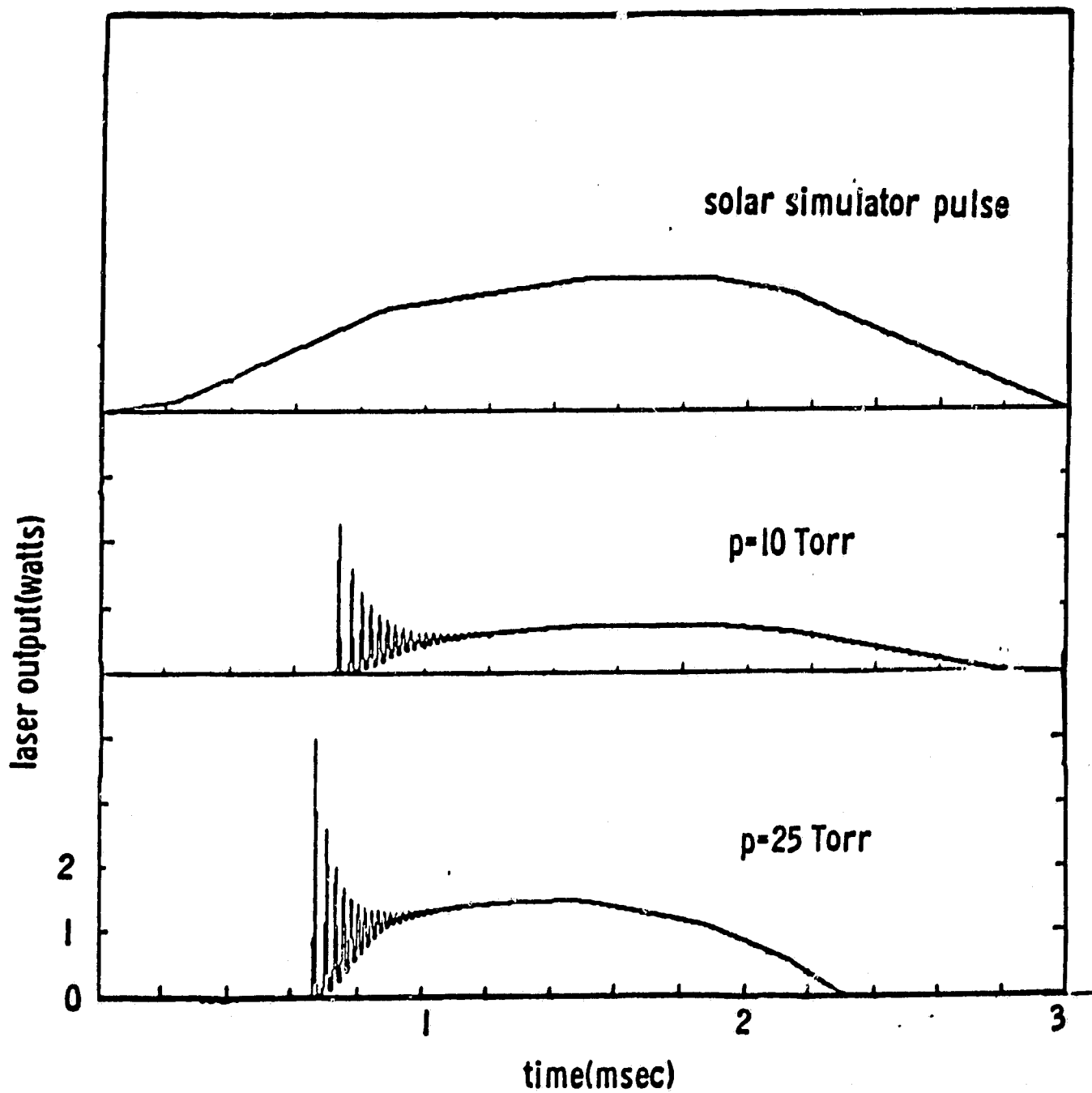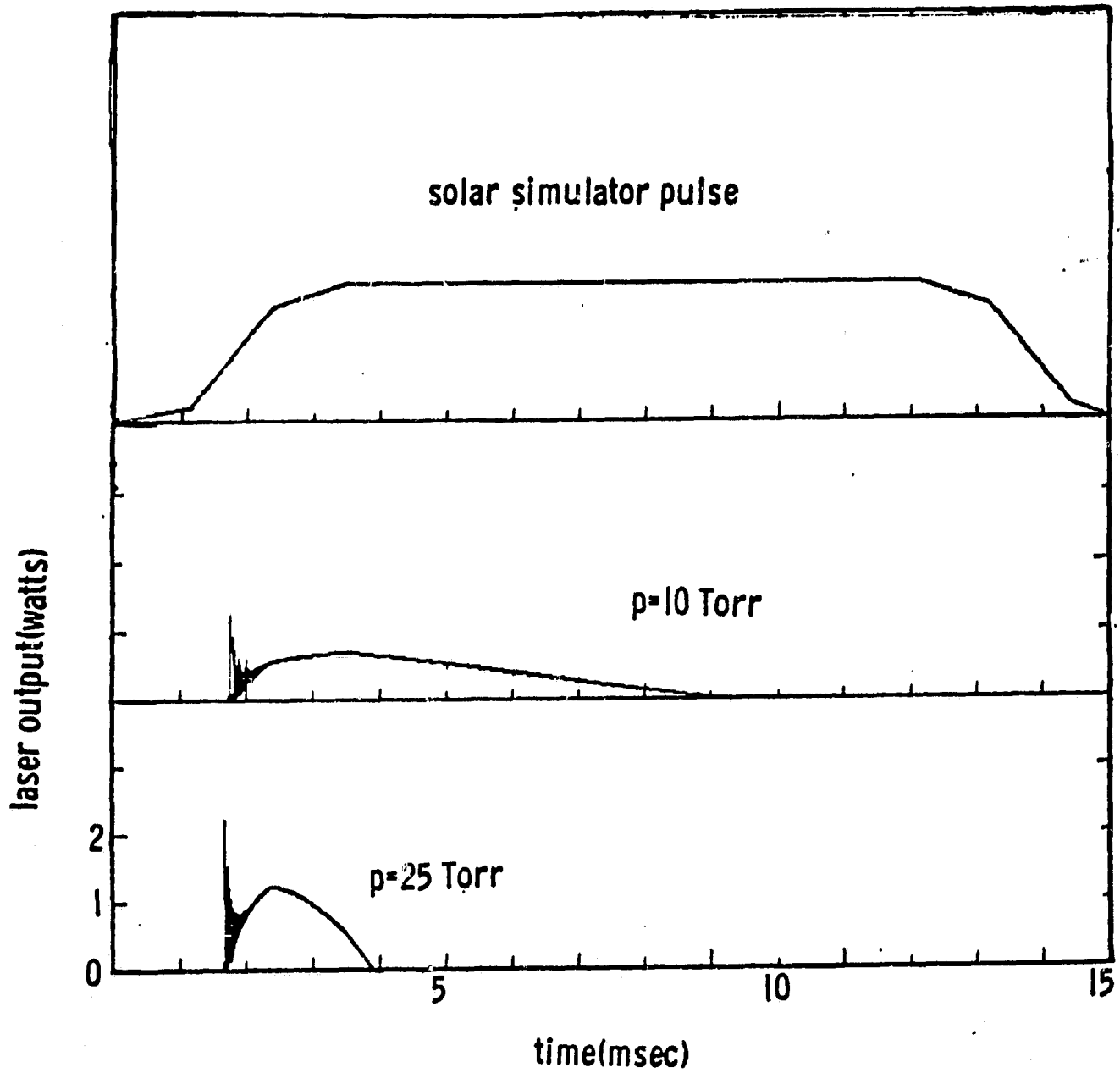
PEAK LASER POWER OUTPUT vs. PRESSURE
WITH OUTPUT MIRROR TRANSMISSION AS PARAMETER
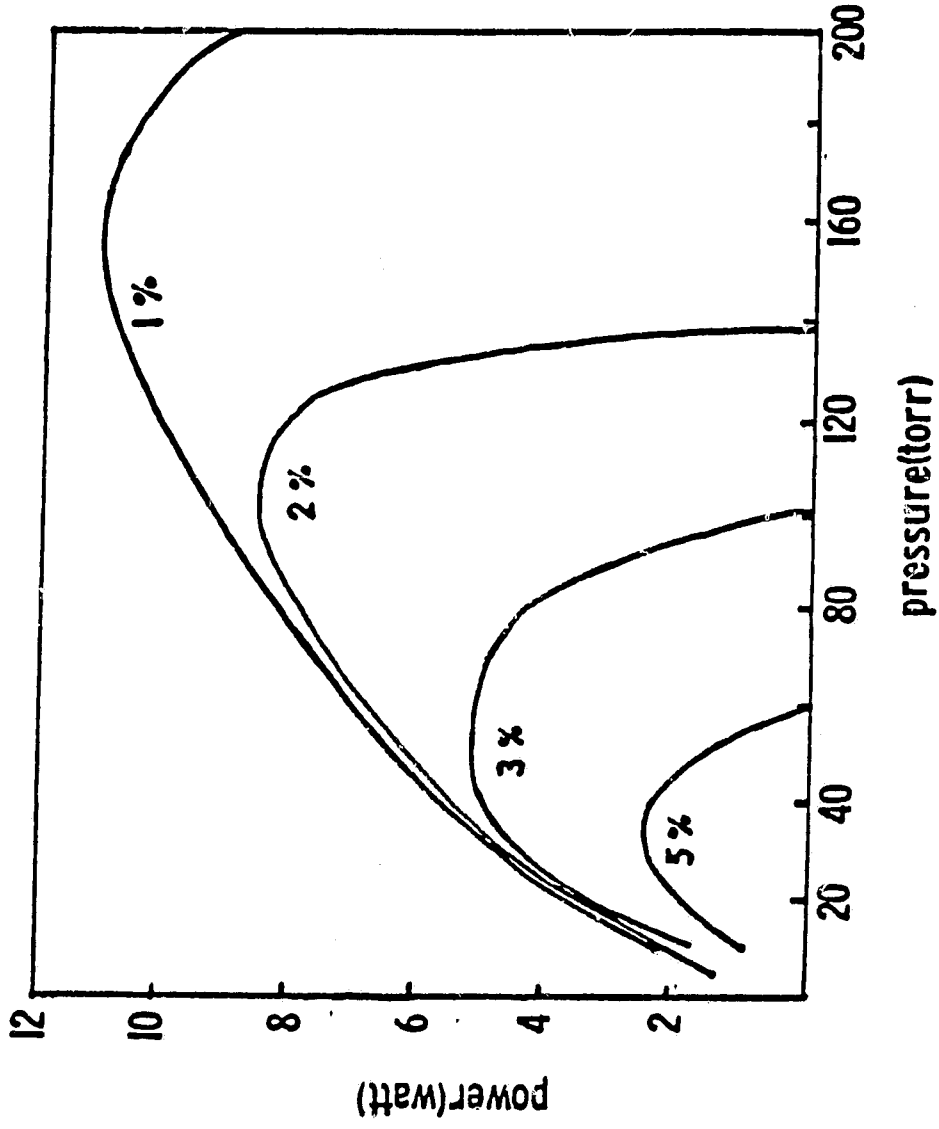
Fig. 14

ENERGY OUTPUT vs. PRESSURE WITH OUTPUT MIRROR
TRANSMISSION AS PARAMETER
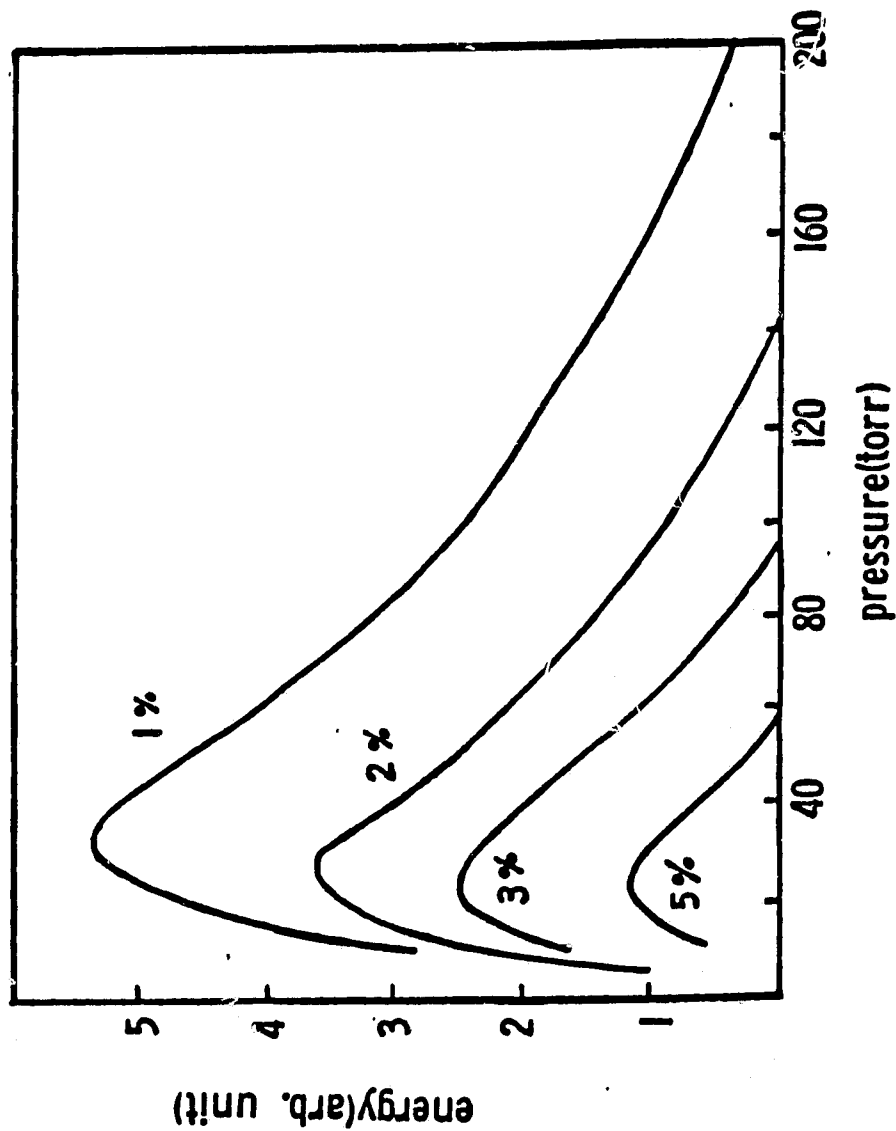
Fig. 15

PEAK LASER POWER OUTPUT vs. SOLAR CONCENTRATION

P=25 torr
2 %T OUTPUT MIRROR
MAX S.C. =14700

fraction of max s.c.

laser output(arb. unit)
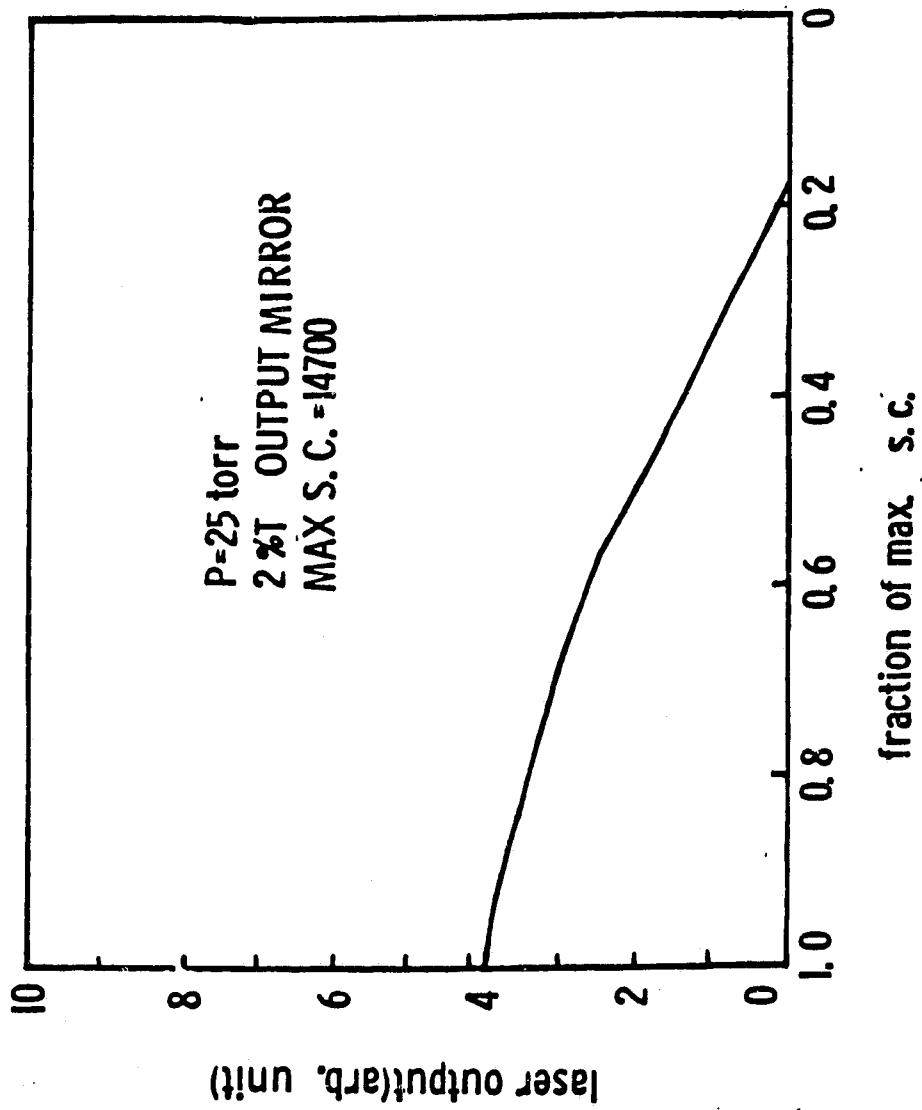
Fig. 16

PEAK LASER POWER OUTPUT vs. OUTPUT MIRROR
TRANSMISSION

P=25 torr

laser output(arb. unit)

transmission(%)
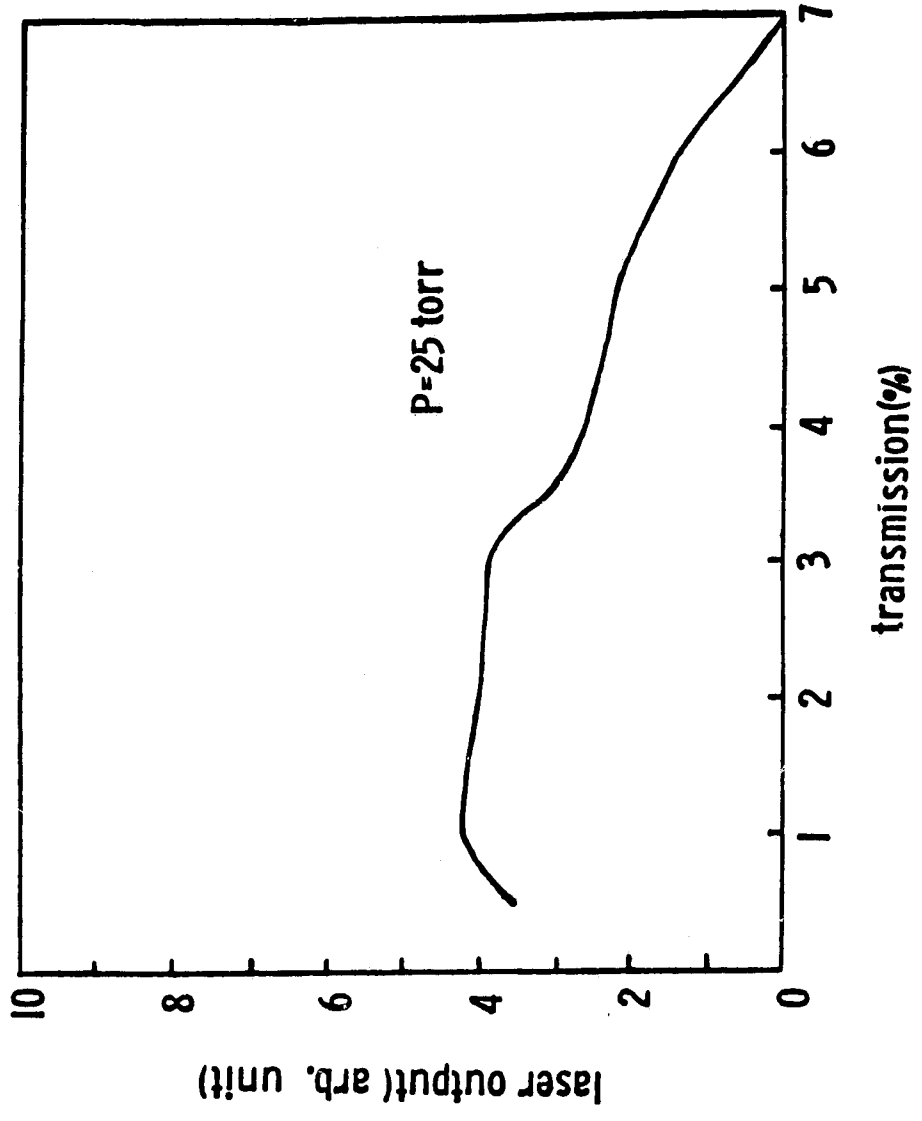
Fig. 17

LASER OUTPUT vs. I$_2$ IMPURITY

P=25 torr
2%T output mirror

energy

peak power

laser output(arb. unit)

I$_2$ impurity(ppm)

Fig. 18

28
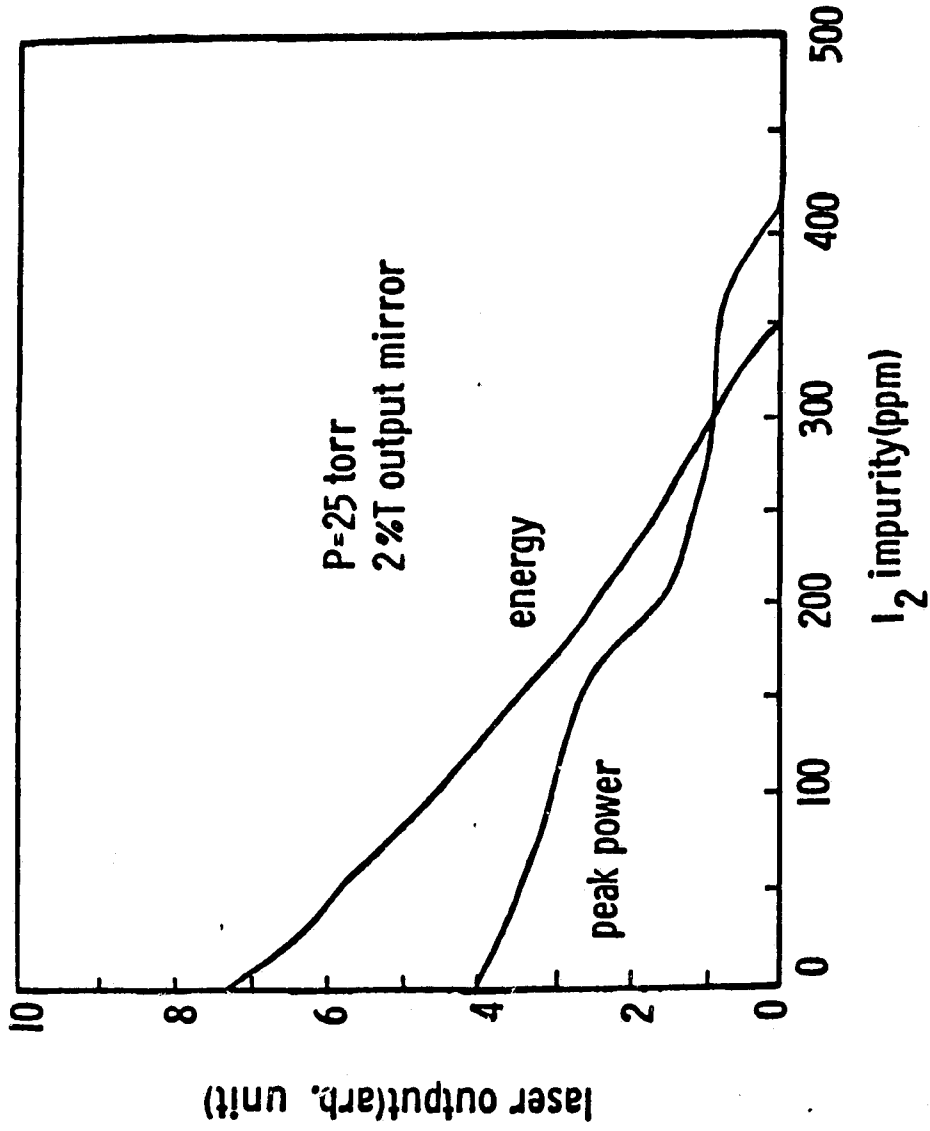
PEAK LASER POWER OUTPUT vs. O₂ IMPURITY

P=25 torr
2 %T OUTPUT MIRROR

laser output(arb. unit)

O₂ impurity(ppm)
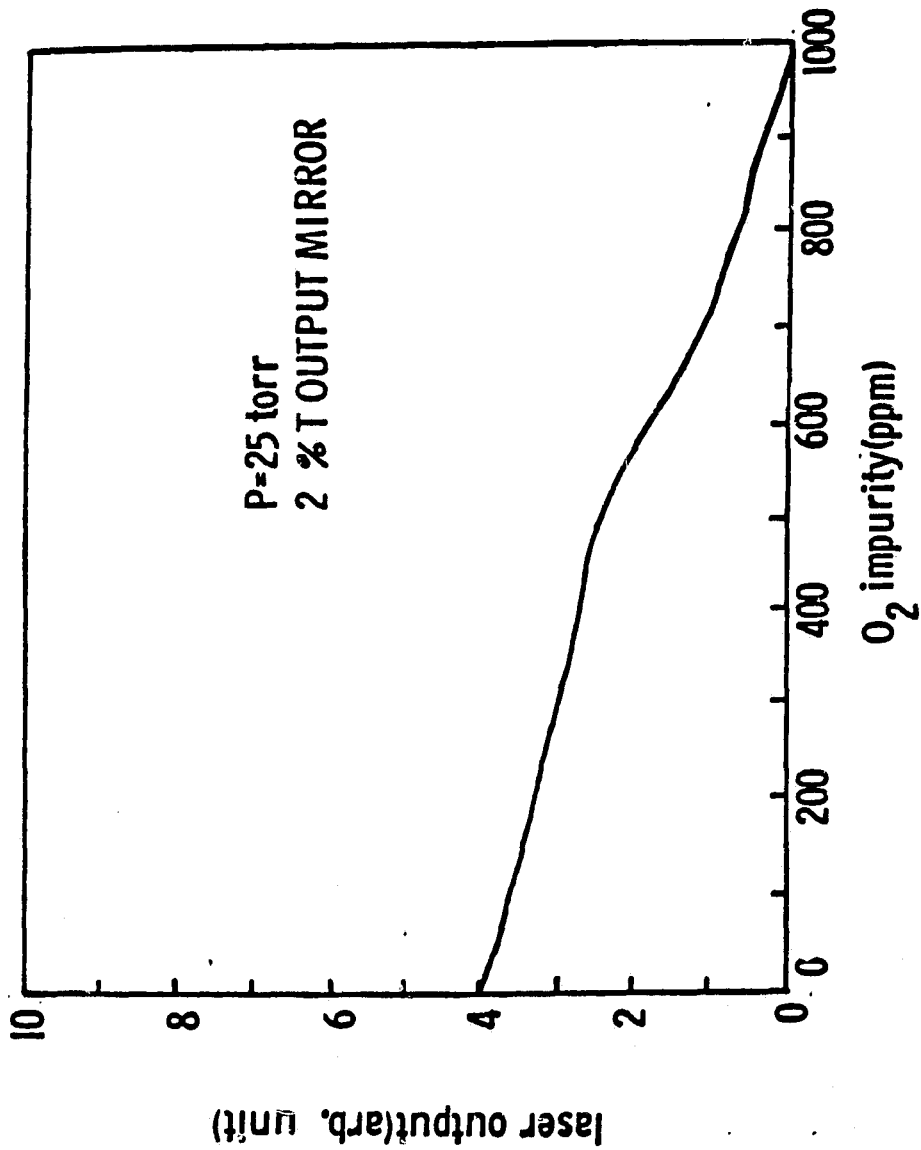
Fig. 19

Fig. 20 LASER OUTPUT WITH SOLAR SIMULATOR PULSE
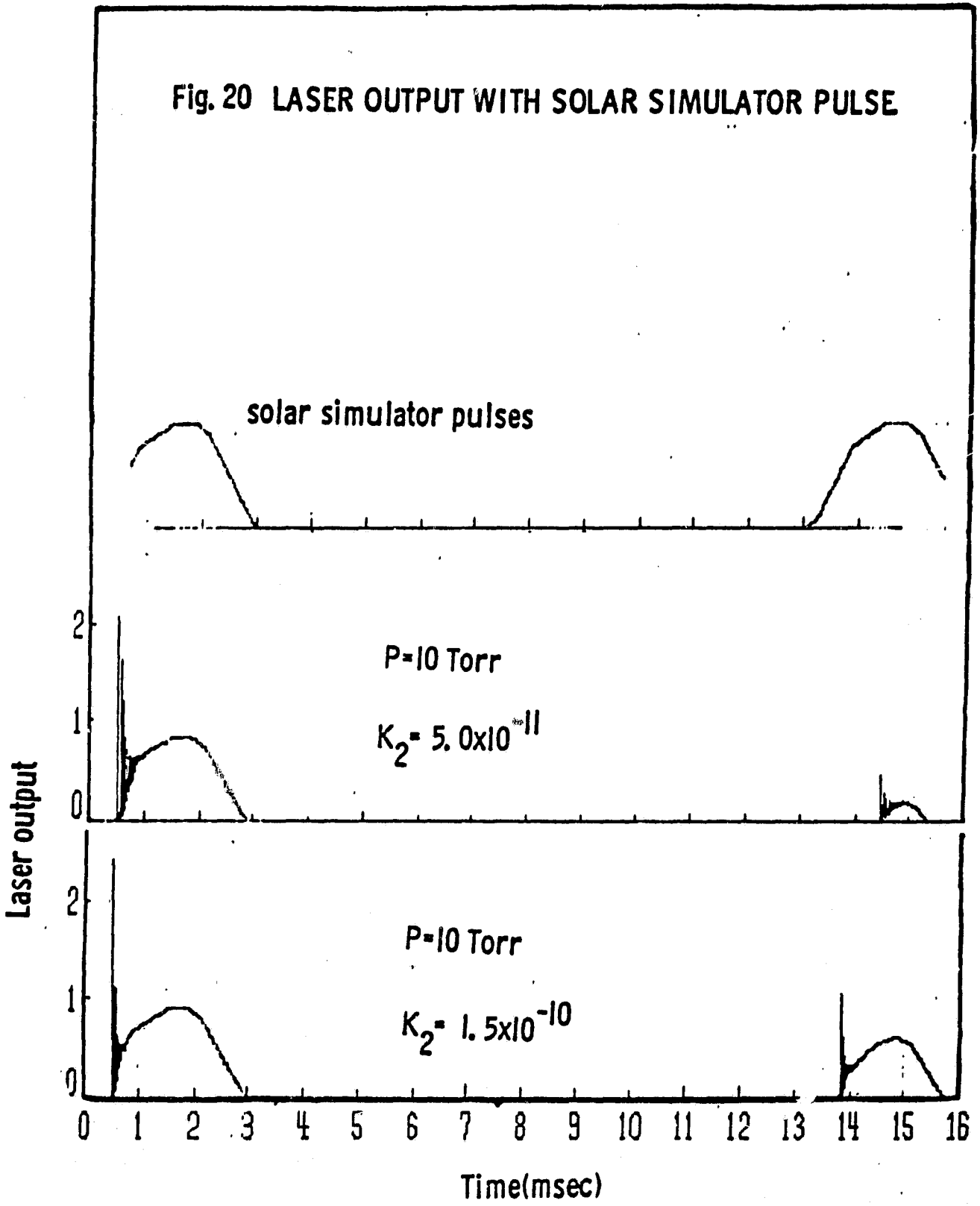
solar simulator pulses

P=10 Torr

$K_2 = 5.0 \times 10^{-11}$

P=10 Torr

$K_2 = 1.5 \times 10^{-10}$

Laser output

Time(msec)

Table I Kinetic Equations

$$\frac{d[RI]}{dt} = K_1[R][I^*] + K_2[R][I] - S_1[RI]$$

$$\frac{d[R]}{dt} = S_1[RI] - K_1[R][I^*] - K_2[R][I] - 2K_3[R][R]$$

$$\frac{d[R_2]}{dt} = K_3[R][R]$$

$$\frac{d[I_2]}{dt} = C_1[I][I^*][RI] + C_2[I][I][RI] + C_3[I][I^*][I_2] + C_4[I][I][I_2]$$
$$- S_2[I_2]$$

$$\frac{d[I^*]}{dt} = S_1[RI] + S_2[I_2] - K_1[R][I^*] - C_1[I][I^*][RI] - C_3[I][I^*][I_2]$$
$$- Q_1[I^*][RI] - Q_2[I^*][I_2] - \Gamma_{23}^7 - A[I^*]$$

$$\frac{d[I]}{dt} = S_2[I_2] + Q_1[I^*][RI] + Q_2[I^*][I_2] + \Gamma_{23}^7 + A[I^*]$$
$$- C_1[I][I^*][RI] - 2C_2[I][I][RI] - C_3[I][I^*][I_2]$$
$$- 2C_4[I][I][I_2] - K_2[R][I]$$

$$\frac{d\rho}{dt} = h\nu \Gamma_{23}^7 - \rho/\tau_c + h\nu Ag[I^*]$$

$$\Gamma_{23}^7 = \omega_{23}\left([I^*] - \frac{[I]}{2}\right)$$

$$\omega_{23} = \lambda^2 A \, c\rho/(4\pi^2 h\nu \Delta\nu)$$

$$\tau_c = -\left(\frac{L}{c}\right) \ln (r_1 r_2)$$

$$g = 2r_b^2/L^2$$

31

Table 2   <u>Rate Coefficients</u>

<u>Reaction</u>	<u>Rate</u>	<u>R</u>	<u>Reference</u>	<u>Symbol</u>	<u>Value-Used</u>
$I^* + R \rightarrow IR$	4(-12)	CF_3	Beverly-Wong	K_1	3.0(-12)
	2.7(-12)	$i\text{-}C_3F_7$	Beverly-Wong		
	1.5(-12)	CF_3	Fisk		
	3.0(-12)	CF_3	LLL		
$I^* + I_2 \rightarrow I + I_2$	3.6(-11)	-	Beverly-Wong	Q_2	3.6(-11)
	3.6(-11)	-	Fisk		
	5(-12)	-	Hohla-Kompa		
	3.2(-12)	-	LLL		
$I^* + RI \rightarrow I + RI$	6.0(-17)	CF_3	Beverly-Wong	Q_1	8.0(-16)
	2.8(-16)	$i\text{-}C_3F_7$	Beverly-Wong		
	4(-16)	CF_3	Hohla-Kompa		
	5.4(-17)	CF_3	LLL		
	8.0(-16)	C_3F_7	LLL		
	4.6(-17)	$n\text{-}C_3F_7$	Stephan-Comes		
$I + R \rightarrow RI$	3(-11)	CF_3	Beverly-Wong	K_2	5.0(-11)
	1.5(-10)	$i\text{-}C_3F_7$	Beverly-Wong		
	5(-11)	CF_3	Fisk		
	5(-11)	CF_3	LLL		
$R + R \rightarrow R_2$	3(-12)	CF_3	Beverly-Wong	K_3	1.1(-12)
	4.2(-12)	C_3F_7	Beverly-Wong		
	8(-12)	CF_3	Fisk		
	6(-13)	$n\text{-}C_3F_7$	Fisk		
	1.5(-13)	$i\text{-}C_3F_7$	Fisk		
	3(-14)	$t\text{-}C_4F_9$	Fisk		

Table 3 <u>COMPARISION OF LASANTS FOR SOLAR LASERS</u>

	C_3F_7I	NOCl	$Br-CO_2$	Dye
threshold inversion density	*10^{14} cm^{-3}	10^{16} cm^{-3}	10^{16} cm^{-3}	high
laser transition	1.3 μm	5-6 μm	2.7,4.3,10.6 μm	*visible
solar spectrum utilization	1.2%, near uv	*40%, uv-6500Å	*15%, visible	visible
Q.E.	*20%	< 10%	<5%	~25%
kinetic	electronic	E-V	E-V transfer	-
high temperature operation	*600K	570K	low	-
chemical reversibility	chemical reprocessing required	slow recovery	*reversible	flowing system

* advantages

Γ_{23} : stimulated emission rate

ω_{23} : stimulation frequency

ρ : intracavity photon energy density

τ_c : lifetime of a photon in the resonator cavity

g : geometric factor for the cavity

$\Delta\nu$: line width

L : length of the laser cavity

r_1, r_2 : mirror reflection coefficients

r_b : laser beam width

S_1 : photodissociation rate coefficient of the iodine compound

$\qquad S_1 = 2.44 \times 10^{-3}$ C sec^{-1} for C_3F_7I at AMO solar irradiance

C : solar concentration

S_2 : photodissociation rate coefficient of iodine

$\qquad S_2 = 4.2 \times 10^{-2}$ C sec^{-1} for I_2

Reaction	Rate	R	Reference	Symbol	Value-Used
$R + R \rightarrow R_2$	1.0(-11)	CF_3	Hohla-Kompa	K_3	1.1(-12)
	1.5(-11)	CF_3	LLL		
	1.0(-11)	C_3F_7	LLL		
$I^* + O_2 \rightarrow I + O_2$	2.5(-11)	-	Burde-McFarlane	-	8.6(-12)
	8.6(-12)	-	LLL		
$I + I + O_2 \rightarrow$ $I_2 + O_2$	3.7(-32)	-	LLL	-	3.7(-32)
$I + I + I_2 \rightarrow 2I_2$	7.4(-32)	-	Beverly-Wong	C_4	2.9(-30)
	3.86(-30)	-	Blake-Burns		
	2.9(-30)	-	LLL		
$I^* + I + I_2 \rightarrow 2I_2$	1.5(-31)	-	Beverly-Wong	C_3	4.3(-32)
	4.3(-32)	-	LLL		
$I + I + RI \rightarrow$ $I_2 + RI$	7.8(-33)	$i-C_3F_7$	Beverly-Wong	C_2	4.5(-31)
	5.2(-33)	CF_3	Beverly-Wong		
	4.5(-31)	$i-C_3F_7$	LLL		
	1.5(-31)	CF_3	LLL		
$I^* + I + RI \rightarrow$ $I_2 + RI$	1.6(-32)	-	Beverly-Wong	C_1	1-6(-33)
	1.0(-33)	-	LLL		
	1.0(-32)	-	Stephan-Comes		

Beverly-Wong,ref.19; Fisk,ref.11; Hohla-Kompa,ref.21; LLL,ref.20;
Blake-Burns,ref.22; Stephan-Comes,ref.23; Burde-McFarlane,ref.24.

CHAPTER II

INTRODUCTION

This chapter summarizes the work done on the iodine laser kinetics from September 1, 1981 through January 31, 1982.

A kinetic model of the iodine laser developed by J.W. Wilson and J.H. Lee has been successful in predicting the threshold and the early pulse structure of the laser output. The experimental results are given in Ref. 2. In this work this model is further developed to include the non-uniform exposure of the laser cell to the pumping light and improved estimates of some of the critical rate coefficients which govern the late time pulse shape are made from the experimental data.

The intensity of the pumping light near the laser tube is given by:

$$C(r,1) = C_0 \; \text{Exp} \left[-2.77 \left(\frac{1^2}{L^2} + \frac{r}{R^2} \right) \right]$$

where $C_0 = 2.7$ kw/cm^2 at the peak of the simulator pulse

$$L = 4.75 \text{ cms}$$
$$R = 0.325 \text{ cms}$$

The effective temperature after reflection from the parabolic mirror was taken as 6000°K and the reflection coefficients of the conic collectors are taken as that for typical $M_g F_2$ coated aluminum surfaces.

The photo-dissociation rates ξ_i of the laser gases are calculated by integration of the photo-absorption cross section over the spectrum of a blackbody at 6000°k. The parameters used for the calculation are given in table I. D_0 is the line width and λ_0 the center of absorption. ξ_is are given by:

$$\xi_i = S_i \left[f \; \text{Exp} \; (-\sigma_0 \; Px) + (1-f) \text{Exp} \; (-0.223 \sigma_0 \; Px) \right]$$

Where P is the alkyliodide partial pressure. x is the depth of penetration

of the pumping light into the laser cell.

The kinetic pathways and the kinetic equations are shown in Fig. 1 and

table II and the kinetic rate coefficients[6-21] are given in table III.

The stimulated emission cross section[13] $\sigma = (2 \times 10^{17} + 0.443 \, R_i)^{-1} \, cm^2$

and the Einstein coefficient[13] $A = 7.7 \, sec^{-1}$. The cavity time constant[22]

$$T = -2 \frac{L_c}{L} \ln r_1 \dot{r}_2.$$

Where L_c is the cavity length (56 cms), and c is the speed of light. r_1, r_2

are reflective coefficients of the cavity mirrors (.995 and .98). P is the photon

density in the optical cavity and g is the coupling parameter of the spontaneous

emission to the optical cavity[1]. g is related to the laser beam width r_b by:

$$g = \frac{2r_b^2}{L^2} = 1.79 \times 10^{-5}$$

The factor $\sqrt{\dfrac{\pi}{2.77}}$ is a geometric factor resulting from the non-uniform

pumping T_{max} is the stimulated emission rate at the spatial peak of the pumping

pulse. Here we are interested in the kinetic processes which dominate in the

laser output at late times. It is found that the shape of the pulse at late times

is governed by the rate at which I_2 is formed, the I_2 quenching coefficient and

recombination rate of I and R.

Specifically it can be shown that the late time pulse depends on the quantity q_2

given by:

$$q_2 = \frac{Q_2 \, C_2}{k_2} \, \varsigma_1 \, [R_i]^2 \, (t - t_{th})$$

From table III it can be seen that the value of $Q_2 C_2 / k_2$ is very uncertain. By

using the laser experimental data at late times, an attempt is made to obtain

limits on the quantity $Q_2 C_2 / k_2$.

37

Fig. 2 shows the laser output pulse when the arc plasma is reasonably steady but there is some motion of the arc plasma after 1.6 msec. Using their laser output pulse, a lower bound on the quantity Q_2C_2/k_2 is derived.

From table III, the rate Constant factor of $n - C_3F_7I$, Q_2C_2/k_2, satifies

$$1.4 \times 10^{-33} \leq \frac{Q_2C_2}{k} \leq 3.4 \times 10^{-30}$$

But the present kinetic model shows that the mean values of table II for Q_2C_2 and k_2 result in excessive quenching so that new limits on these parameters can be set by the present experiments as shown in table IV. The new limits are:

$$1.4 \times 10^{-33} \leq \frac{Q_2C_2}{k_2} \leq 1.9 \times 10^{-31}$$

In Fig. 1, the experimental laser output as seen by the germanium detector is compared to the calculated laser output for $k_2 = 2.3 \times 10^{-11}$, $Q_2 = 4.4 \times 10^{-11}$ $C_2 = 6.9 \times 10^{-32}$.

Table IV also shows the kinetic rates associated with other experiments. k_2 lies midway between the previously reported values which differed by an order of magnitude. The earlier values of Q_2 (ref 9 and 15) must be reflected on the basis of the present results while more recent is consistant with the present result.

The latest kinetic results in detail will be found in NASA Technical Paper 2182.

REFERENCES

1. J. W. Wilson, and J. H. Lee, Va. J. Sci. 31, 34 (1984).

2. J. H. Lee, and W. R. Weaver, Appl. Phys. Lett. 39, 137 (1981)

3. J. B. Koffend, and S. R. Leone, Chem. Phys. Lett. to be published.

4. S. R. Leone, Molecular Photofragmentation Precesses Related to Solar-Pumped Gas Laser Development, Seminannual Report, NAG- 1-170, April-Sept. 1981.

5. K. R. Wilson, Photofragment Spectroscopy of Dissociative Excited States, Chpt. 2 of Excited State Chemistry, Ed. by J. N. Pitts, Gordon and Breach, NY (1970).

6. C. E. Turner and N. L. Rapagnani, Laser Fusion Program-Seminannual Report, UCRL-50021-73-1, UCID-16935 (Jan-June 1973).

7. S. V. Kuznetsova, and A. I. Maslov, Sov. J. Q. E. 3, 468, (1975)

8. R. E. Beverly, and M.C. Wong, Optics Commun. 20, 3 (1977).

9. S. V. Kuznetsova, and A. I. Maslov, Sov. J. Q. E. 8, 906, (1978).

10. G. A. Skorobagatov and O. N. Slesar, Bull. Leningrad Univ. 1, 39 (1979).

11. G. A. Skorobogator, V. S. Komarov, and V. G. Seleznev, Sov. Phys. Tech Phys. 19, 1239 (1975).

12. G.A. Fisk, The Effects of Chemical Kinetics and Starting Material Regeneration on the Efficiency of an Iodine Laser Amplifier. Sandia Report SAND77-0990 (1977).

13. K. Hohla, and K. L. Kompa, The Photochemical Iodine Laser, Chpt. 12 Handbook of Chemical Lasers, Ed. by R. W. F. Gross and J. F. Bott, Wiley and Sons NY (1976)

14. S. K. H. Stephens, and F. J. Comes, Chem. Phys. Lett. 65, 251 (1975).

15. R. J. Donavan, and D. Hussain, Nature 171, 4960 (1965).

16. V. A. Kartazaev, N. P. Pekin, and Yu. A. Tolmachev, Sovl J. W. E. 7, 608 (1977).

17. G. E. Busch, IEEE J. Q. E., QE-17, 1128 (1981).

18. I. Arnold, F. J. Comes, and S. Pointech, J. Chem. Phys. 9, 237 (1975)

19. H. Hofmann, and S. R. Leone, J. Chem. Phys. 69, 643 (1978).

20. D. Bunker, and N. Davidson, J. Amer. Chem. Soc. 80, 5058 (1958).

21. J. A. Blake, and G. Burns, J. Chem. Phys. <u>54</u>, 1480 (1971).

22. B. A. Lengyel, Introduction to Laser Physics, Wiley and Sons, NY (1966).

23. J. W. Wilson, S. Raju, and Y. J. Shieu, Solar Simulator-pumped Atomic Iodine Laser Kinetics NASA TM 2182 (1983)
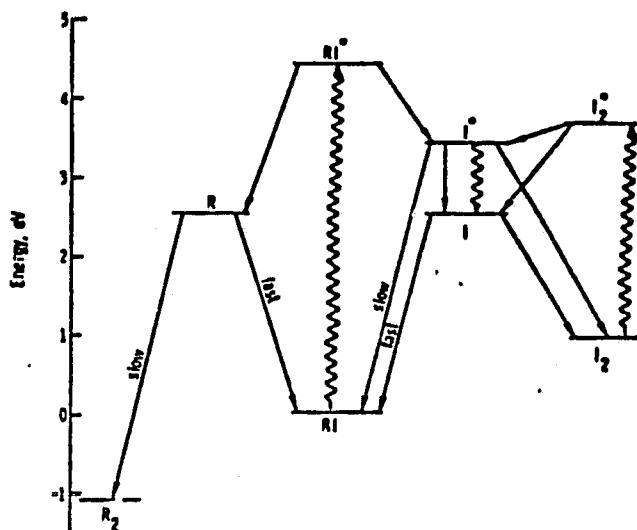
Fig. 1. Energy level diagram of the alkyliordide photo-
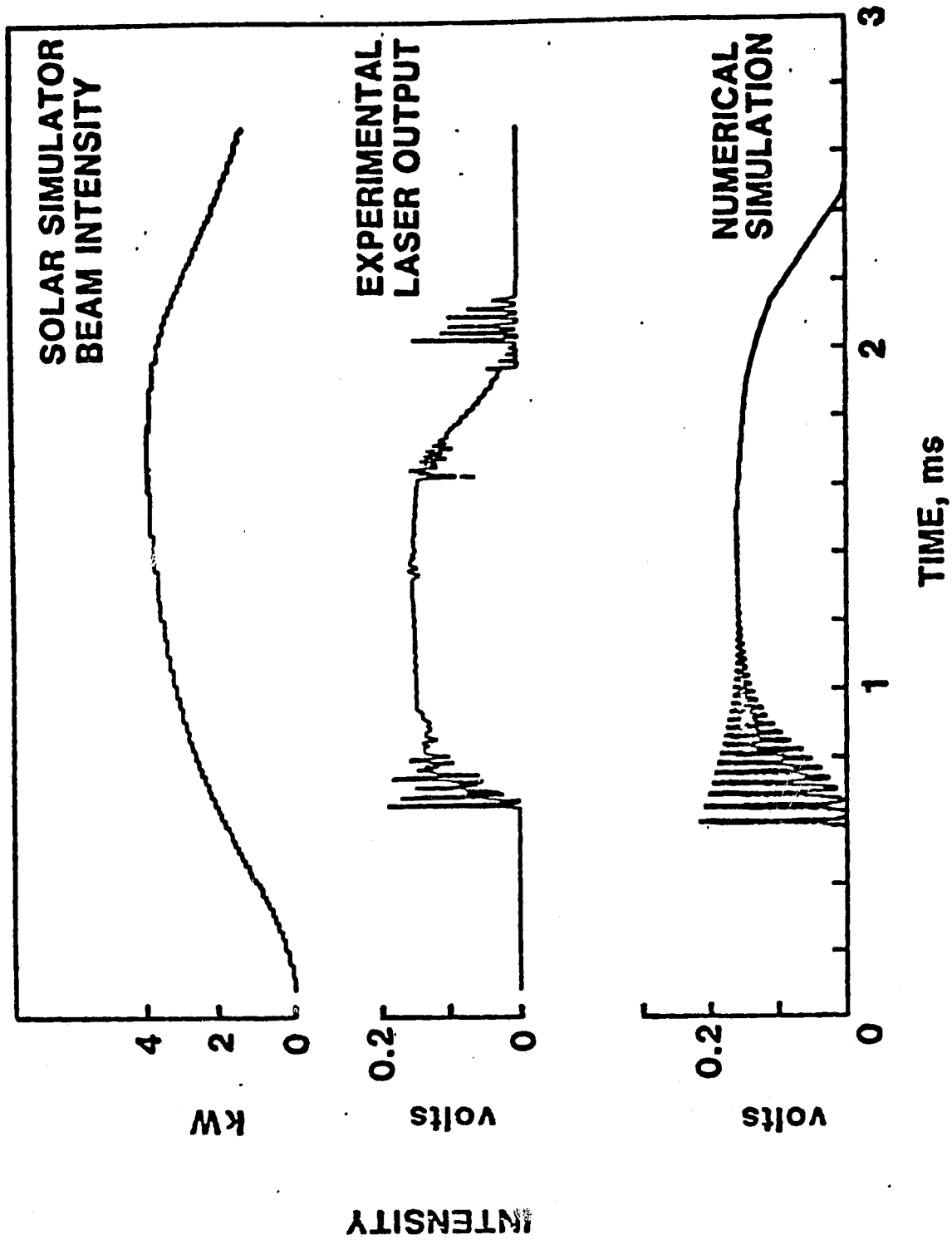chemical Laser showing kinetic pathways.

41

Fig. 2. Beam Intensity of Solar simulatory Experimental
Laser Output and Numerical Simulation as a
function of time.

Table I. Photodissociation parameters used for the equivalent power of one solar constant exposure $C_0 = (1.4 \text{ kW/m}^2)$.

	$n\text{-}C_3F_7I$	$i\text{-}C_3F_7I$	I_2
σ_0, cm^2	7.9×10^{-19}[a]	6.2×10^{-19}[b]	9.14×10^{-19}[c]
λ_0, nm	272[a]	275[b]	499[c]
D_0, nm	12.7[a]	14.5[b]	23.0[c]
ϕ_{I^*}	1.0[a]	1.0[b]	0.51
S, sec^{-1}	3.04×10^{-3}	3.37×10^{-3}	3.38×10^{-2}
f	0.652	0.653	0.673

[a]ref. 3
[b]ref. 4
[c]ref. 5

Table II. Kinetic Equations

$$\frac{d[Ri]}{dt} = K_1[R][I^*] + K_2[R][I] - \left(\frac{R_{uv}}{R_{vis}}\right)\xi_1[Ri]$$

$$\frac{d[R]}{dt} = \left(\frac{R_{uv}}{R_{vis}}\right)\xi_1[Ri] - K_1[R][I^*] - K_2[R][I] - 2K_3[R]^2$$

$$\frac{d[R_2]}{dt} = K_3[R]^2$$

$$\frac{d[I_2]}{dt} = C_1[I][I^*][Ri] + C_2[I]^2[Ri] + C_3[I][I^*][I_2]$$

$$+ C_4[I]^2[I_2] - \xi_2[I_2]$$

$$\frac{d[I^*]}{dt} = \left(\frac{R_{uv}}{R_{vis}}\right)\xi_1[Ri] + \xi_2[I_2] - K_1[R][I^*] - C_1[I][I^*][I_2]$$

$$- C_3[I][I^*][I_2] - Q_1[I^*][Ri] - Q_2[I^*][I_2] - \Gamma_{max} - A[I^*]$$

$$\frac{d[I]}{dt} = \xi_2[I_2] + Q_1[I^*][Ri] + Q_2[I^*][I_2] + \Gamma_{max} + A[I^*]$$

$$- C_1[I][I^*][Ri] - 2C_2[I]^2[Ri] - C_3[I][I^*][I_2]$$

$$- 2C_4[I]^2[I_2] - K_2[R][I]$$

$$\frac{dp}{dt} = \Gamma_{max}\sqrt{\frac{\pi}{2.77}}\frac{\ell}{L_c} - \frac{1}{\tau_c}p + gA[I^*]$$

$$\Gamma_{max} = c\sigma\, p\left([I^*] - \frac{1}{2}[I]\right)$$

44

Table III. Mean kinetic coefficients obtained from the literature and the associated uncertainty factors. Note that the factor in parenthesis give the uncertainty limits associated with each rate.

	$n\text{-}C_3F_7I$	$i\text{-}C_3F_7I$
K_1[a]	$7.9 \times 10^{-13} (5.9)^{\pm 1}$	$4.4 \times 10^{-13} (5.4)^{\pm 1}$
K_2[b]	$2.3 \times 10^{-11} (3.5)^{\pm 1}$	$3.9 \times 10^{-11} (4.3)^{\pm 1}$
K_3[c]	$2.6 \times 10^{-12} (4)^{\pm 1}$	$9.0 \times 10^{-13} (3.8)^{\pm 1}$
Q_1[d]	$2.0 \times 10^{-16} (4.2)^{\pm 1}$	2.8×10^{-16}
Q_2[e]	$1.9 \times 10^{-11} (2.6)^{\pm 1}$	$1.9 \times 10^{-11} (2.6)^{\pm 1}$
C_1[f]	1×10^{-33}	$8.8 \times 10^{-33} (1.2)^{\pm 1}$
C_2[g]	$8.5 \times 10^{-32} (5.3)^{\pm 1}$	$8.3 \times 10^{-32} (5.3)^{\pm 1}$
C_3[h]	$5.6 \times 10^{-32} (1.5)^{\pm 1}$	$5.6 \times 10^{-32} (1.5)^{\pm 1}$
C_4[i]	$2.0 \times 10^{-30} (4.3)^{\pm 1}$	$2.0 \times 10^{-30} (4.3)^{\pm 1}$

[a]refs. 6-10
[b]refs. 6-11
[c]refs. 6-12
[d]refs. 6, 7, 13, 14
[e]refs. 6, 8, 12, 13, 15-19

[f]refs. 6, 8, 14
[g]refs. 6-8
[h]refs. 6, 8
[i]refs. 6, 8, 17, 20, 21

Note that the factor in parenthesis give the uncertainty limits associated with each rate.

Table 1V. Present values for late time kinetic rate coefficients in comparison to previous estimates.

	Present	Others
K_2	4.3×10^{-11} $(1.9)^{\pm 1}$	$8.5 \times 10^{-11})$[a] $9.0 \times 10^{-12})$[a] $7 \times 10^{-12})$[b]
Q_2	3.1×10^{-11} $(1.6)^{\pm 1}$	$5 \times 10^{-12})$[c] $3.2 \times 10^{-12})$[d] $2.1 \times 10^{-11})$[e] $3.1 \pm .5 \times 10^{-11})$[f]
C_2	3.7×10^{-32} $(2.3)^{\pm 1}$	$8.5 \times 10^{-32})$[a]

[a]ref. 7
[b]ref. 9
[c]ref. 15
[d]ref. 6
[e]ref. 16
[f]refs. 8, 17, 18, 19

Chapter IV   Direct-Solar-Pumped Laser Amplifier

1. Introduction

This part of the report summarizes the research performed during March 1, 1983, through February 29, 1984. Our major effort was in evaluating the concept of a direct solar-pumped laser amplifier using 2-iodohepafluoropropane ($i-C_3F_7I$) as the laser material. To simulate the solar radiation in space with a pulsed flashlamp light, we measured the spectral distribution of emission from a long flashlamp. We also developed a parabolic cylindrical reflector-collector system in which the beams from the flashlamp are projected parallel resulting in a beam profile similar to that of the solar beam. We measured the optical energy coupling efficiency by the reflector-collector system from the flashlamp into the laser tube using a modified photodiode detector. Also measured is the optimum pressure of the $i-C_3F_7I$ gas in the laser tube for the present pumping scheme. It was found that the optimum pressure of the $i-C_3F_7I$ gas in the laser tube was about 30 torr for the input energy of 135 J. The threshold inversion density of the laser was calculated from the experimental data of the pumping light and the optimum pressure inside the laser tube. The laser cavity was composed of 99.8-percent R and 98-percent R mirrors.

We estimated the photodissociation rate from the measured threshold condition. The photodissociation rate was about 0.05 percent of the $i-C_3F_7I$ molecules for the electrical energy of 135 J applied to the flashlamp. This photodissociation rate is directly connected to the energy storage capacity of the laser tube to be used as an amplifier tube. Further investigation on the amplifier scheme is currently pursued under a new NASA grant.

2. Iodine laser

We used $i-C_3F_7I$ gas as a laser material for the direct solar-pumped laser

although the i-C_3F_7I is far from being an ideal laser material for the solar-pumped laser, because of the poor overlap between the absorption band of the i-C_3F_7I and the solar spectral distribution. However, among the many laser schemes, such as an iodine photodissociation laser [1], an iodine bromide photodissociation laser [2], a neodymium chelate laser [3], and a blackbody pumped laser [4], only the iodine photodissociation laser has been successfully demonstrated with a solar simulator because it has excellent laser kinetics for a high power laser. After the laser action in atomic iodine produced by photodissociation of alkyliodide was discovered [5], it was considered as one of the candidates for the inertial confinement or laser fusion driver [6]. Extensive studies were followed for topics such as (1) lasing process, (2) spectroscopic structure of laser transition, (3) power and energy amplification, (4) parameters in kinetic process, (5) development of efficient laser materials, and (6) effective pumping methods. From the results of many researchers, it is known that i- or n-C_3F_7I is the most effective laser material. When these chemical compounds (parent molecules) are irradiated by ultraviolet (UV) radiation (250 - 300 nm), these molecules are dissociated into excited atomic iodine (5 $^2P_{1/2}$) and perfluoroalkyl radical R (R = i-C_3F_7I or n-C_3F_7). The excited atomic transits to ground state (5 $^2P_{1/2}$) causing laser excitation at the wavelength of 1.3 µm as shown in figure 1. However by the influence of the nuclear magnetic moment of the atomic iodine, the upper level of the transition is split into two sublevels and the lower level of the transition is split into four sublevels [7]. These sublevels are designated by F number as shown in figure 2. Because of this hyperfine struture, the laser transition and amplifying processes are rather complicated. The transition probability from F = 3 of the upper level to F = 4 of the lower level is the highest, so that, in most cases, the laser oscillation comes from this transition.

The excited iodine atoms have a very long lifetime because their electric dipole transitions from the upper states to the ground states are forbidden. Only the magnetic dipole or electric quadruple transition is allowed, so that the transition probability is very low. Both calculated [8] and measured [7, 9] lifetimes of the excited iodine atom extend more than 100 ms. This lifetime of the excited iodine atom allows the laser oscillation by a weak pumping power such as moderately-concentrated solar power.

Another advantage of the i-C_3F_7I photodissociation laser is the high degree of reversibility of the chemical processes. It is known that more than 90 percent of the used chemical in the laser oscillation can be recombined to its original compound [10]. This characteristics of the i-C_3F_7I allows quasi-sealed-off operation of the iodine laser. But, this chemical has a disadvantage for solar-pumped laser application, because the power of the near UV band from the solar radiation useful for photodissociation of the i-C_3F_7I is only 1 percent, as mentioned earlier.

As shown in figure 1, the laser action by the photodissociation of the perfluoroalkyl iodide is very complicated and various physical and chemical reactions are involved in the iodine laser action. Many researchers were engaged in determining the reaction constants [11, 12], yet the experimental data of the reaction constants scatter over a wide range among the researchers. Theoretical works have also been performed for understanding of the solar-pumped laser kinetics based on the experimentally determined reaction constants [13,14, 15]. Recently, J.W. Wilson et al. [16] have studied various reaction constants already published, and they investigated threshold kinetics of solar-simulator-pumped iodine laser and found general agreement with experimental results of Langley Research Center. This work may be extended to the amplifier system for better understanding of our experimental results.

3. Laser System

The laser system used in this experiment is shown in figure 3. We used two parabolic aluminum (ALZAK finish) cylinders to compose a reflector-collector system of flashlamp light to simulate the solar beam in space. The non-parallel beam from the flashlamp was filtered out by installing a narrow, circular cylinder in front of the flashlamp (see fig. 3). The flashlamp was located at the focus of the parabolic cylindrical reflector. The laser tube was made of a quartz tube with 15 mm O.D. and 11.5 mm I.D. The pumped length of the laser tube was 116.5 cm.

The windows of the laser tube, which were made of INFRASIL, were installed on a pair of demountable connectors at Brewster's angle. The demountable connectors make cleaning the system easy after successive operations of the laser excitations. It is necessary to remove the iodine crystals, some solid photochemical products, and dust which adhere inside the tube and on the Brewster's windows.

The optical cavity was composed of a fully-reflecting mirror (R = 99.8 percent) with a radius of curvature of 10 m and a partially-reflecting mirror (R = 98 percent) as an output coupler. At times, a partially-reflecting mirror, with 85 percent reflectance, was used as an output coupler.

The gas supply system is shown in figure 4. Prior to filling the i-C_3F_7I gas into the laser tube, the laser tube was evacuated down to 2×10^{-6} torr with the high vacuum system. The i-C_3F_7I gas was distilled under vacuum by cooling one evacuated bottle with liquid N_2 and keeping the i-C_3F_7I liquid around $-20^\circ C$.

The gas fill pressure in the laser tube was measured by an MKS Baraton pressure gage (Head, 2154; signal conditioner, 2155; power supply, 2156).

4. Measurement of the peak spectral power distribution of flashlamp

The flashlamp used in this experiment was ILC-4855, which had 5 mm I.D., and the arc length was about 120 cm. The electrical circuit used for energizing the flashlamp is shown in figure 5. The main energy-storage capacitor had capacitance of 2.7 μF and could be charged to 30 kV. The electrical energy applied to the flashlamp was varied by the charging voltage of the storage capacitor.

The trigger pulse was applied to the spark gap and to the flashlamp simultaneously, to obtain reliable and prebreakdown-free operation of the flashlamp for a wide range of the charging voltage of the storage capacitor.

At first, the absolute spectral-power-output characteristics of the flashlamp was measured to compare with the solar radiation. The measurement of the peak spectral-power-output distribution from the flashlamp was carried out by comparing with the spectral-power distribution of a standard carbon-arc light source. The spectral-power-output distribution of the carbon arc was measured by others and it is known that the spectral-power-output distribution of the carbon arc, operated under specified conditions, is very reliable for the absorption band of $1-C_3F_7I$ (250 nm ~ 300 nm)[16, 17]. A Bogen-Lampe made by Spindler-Hoyer Company was used for this purpose. The electrodes of the carbon arc were Noris H carbon rod (dia., 6 mm) for the anode, and Noris D carbon rod (dia., 7 mm) for the cathode. The arc current was fixed at 7.4 A. The light from the carbon arc was chopped by an optical chopper at the frequency of 670 Hz. Using a spectrometer (McPherson 0.5 m) and a photomultiplier (P.M.) tube (EMI 9659 QB), the optical intensity from the carbon arc was measured at every 10 nm from 240 nm to 500 nm. The spectrometer was equipped with a grating having 600 lines/mm, and the grating was blazed at 300 nm.

The light intensity of the flashlamp was also measured at every 10nm to compare with that of the carbon arc. To make the same solid angle of emission from the two light sources, the identical optical system was placed at the same distance from the sources. The measuring system is described in figure 6.

By comparison of the peak light intensities by the monochromator-P.M. tube system for the carbon arc and the flashlamp at each wavelength, we obtained the results shown in figure 7. When the charging voltage of the storage capacitor for the flashlamp was 10 kV (electrical energy; 135 J), the peak spectral-power output in the pumping band of $i-C_3F_7I$ was comparable to that of the 6,000 K blackbody radiator.

The spectral energy distributions of the carbon arc and the flashlamp were also recorded on the photographic film (Kodak tri-X pan film). The densitometric traces are shown in figure 8. The upper four traces are for the spectral output energy from the standard carbon arc at different exposure times. The exposure time was determined by using a well-calibrated optical shutter. The lower four traces are for the spectral output energy from the flashlamp at different electrical energies. By using the upper four traces, the contrast index (C.I.) of the used film could be determined by the relation

$$\frac{D - D_O}{\log E - \log E_O} = \gamma \tag{1}$$

for the linear region of the optical density (D) of the exposed film. The E in equation (1) is known as exposure and is the amount of the exposed spectral energy to the film. If we plot the optical density versus the logarithm of the exposure, we could obtain the H-D curve (Hunter-Driffield curve) as shown in figure 9. At the wavelengths of 260 nm, 270 nm, 280nm, and 290 nm, the measured optical densities of the film have shown a good linearity against

52

the logarithm of the exposures and the measured C.I. was unity. However, at the wavelength 250 nm, the optical density of the film is not linearly dependent on the logarithm of the exposure because of the weak exposure. And, at the wavelength 300nm, the film is saturated at the long exposure time so that the optical density is also not linearly dependent on the exposure.

If the C.I. of the film is determined, then the spectral-radiant energy can be calculated from equation (1), i.e.,

$$E = E_0 10^{(D-D_0)/\gamma} \tag{2}$$

By using the spectral-radiant energy of the carbon arc for 0.1 second exposure as the reference spectral-radiant energy, the spectral-radiant energy from the flashlamp was obtained. The spectral-power distribution of the flashlamp could be calculated by dividing the spectral-radiant energy of the flashlamp derived from equation (2) by the measured optical pulse width. The spectral-power distribution measured by the monochromator-P.M. tube method is compared in table 1 to that measured by the densitometric method. However, the comparison of the results in table 1 shows that the measurement of the spectral-power distribution by the densitometric traces are up to 100 times larger. This discrepancy is resulted from the poor reciprocity of the photographic film used in this experiment [18]. So, the quantitative relation obtained by the densitometric method is unreliable.

Table 1.—Comparision of the peak spectral power output measured by two different methods.

Wave-length nm	Monochrometer-P.M. tube method Unit; w/cm^3 sterad			
	135.0 J	210.9 J	303.8 J	413.4 J
260	1.01×10^7	1.64×10^7	2.02×10^7	2.20×10^7
270	0.71×10^7	1.21×10^7	1.61×10^7	1.19×10^7
280	1.44×10^7	2.03×10^7	2.44×10^7	2.87×10^7
290	1.96×10^7	3.15×10^7	3.88×10^7	4.57×10^7

Wave-length nm	Densitometric method			
	135.0 J	210.9 J	303.08 J	413.4 J
260	3.31×10^8	5.75×10^8	1.00×10^9	2.22×10^9
270	4.10×10^8	7.54×10^8	1.11×10^9	2.46×10^9
280	3.75×10^8	6.52×10^8	1.02×10^9	2.12×10^9
290	3.26×10^8	6.36×10^8	1.86×10^9	1.31×10^9

5. Measurement of Coupling Efficiency of Pump Light

When the flashlamp is energized, the light emitted from the flashlamp is focused into the axis of the laser tube through the quartz tube by reflection from the reflector-collector system (see fig. 3). However, because of imperfectness of both the reflectance of the aluminum reflectors and the transmittance of the quartz tube, the optical energy from the flashlsp cannot be coupled into the laser tube. Moreover, because of our intention to simulate the near-parallel solar-beam profile by using parabolic, cylindrical reflectors, the pumping intensity in the laser tube became anisotropic. So, it was necessary to measure the coupled energy into the laser tube from the flashlamp.

To measure the coupling efficiency of the optical energy in the UV range, the best instrument is a P.M. tube which has a good sensitivity in UV light. But, a P.M. tube which can be installed in our laser tube (I.D., 11.5 mm) was not available. To avoid this difficulty, a small detector system was made of a silicon photodiode (EG&G, SGD-040A), as described in figure 10. By the previous measurement, we found that the optical pulse shape from the flashlamp in visible and UV range was rather different from that in I.R. range. So, a glass filter which cut the I.R. light was used in front of the silicon photodiode, such that the detector system had no I.R. response. The transmittance of the used glass filter is shown in figure 11. The range of ≥ 50 percent transimission lies between 385 nm and 540 nm. The photodiode was biased 90 V negatively, and the signal cable was terminated by a 50Ω resistor.

By using a set of neutral density filters, the linearity of the detector system was examined. The detector response to the optical intensity is shown in figure 12. As shown in figure 12, the response of this detector is linear up to 18 mA, which corresponds to 900 mV for 50Ω termination. Therefore, all measurements were taken below this limit.

After the examination of the detector response, the optical intensities
at different distances from the flashlamp for different applied electrical
energies were measured. By these measurements, the optical intesnsity at the
distance 0.5 cm from the flashlamp axis were extrapolated, so that the light
intensity at 0.5 cm from the laser tube axis could be compared. These measurements
were best fitted by the curve

$$I = [I_o/r] \times [1 - \exp(-r/1.70)] \quad\quad\quad (3)$$

as shown in figure 13, where r is the distance of the detector from the flashlamp
axis. This result is reasonable based on the physical consideration of the
measurement. Since the flashlamp is very long (120 cm arc length) so that it can
be approximated to a line source if the detector is located far from the lamp.
The optical intensity from the linear light source is proportional to the inverse
of the distance. However, as the position of the detector comes closer to the
flashlamp the inverse distance relation for the optical intensity needs short
range correction. This correction appears in equation (3) as $[1 - \exp(-r/1.70)]$.

The optical intensity coupled into the laser tube was measured by inserting
the same detector into the laser tube. The optical intensities were measured at
six different positions along the axis of the laser tube and at every 15° around
the tube axis. After the measurements of the photodetector signals of the optical
intensities, they were compared with the detector signal extrapolated by equation
(3) to the distance 0.5 cm away from the flashlamp axis. The results are shown
in figure 14. Because of the parabolic geometry of the reflector-collector system,
the optical intensities coupled into the laser tube in the direction of 0° and
180° of the focal plane are very weak. Also the optical intensity distribution
around the tube axis is very irregular and, except for the middle part of the

laser tube, the intensity distribution is quite asymmetric. This irregularity and asymmetry may be originated from the imperfectness of the narrow, circular cylinder which reflects back the nonparallel beam from the flashlamp (see fig. 3).

The results shown in figure 14 are the optical intensity coupling efficiencies in the visible range (~ 475 nm) of the spectrum. To convert these results into the UV range (~ 270 nm) of the spectrum, we should consider the path of the beam. Referring to figure 3, most of the beam from the flashlamp is to reflect from the reflector-collector system to be coupled into the laser tube. The reflectance of the aluminum sheet used for the reflector-collector system in the UV range of the spectrum is about 70 percent of that in the visible range [19]. Including this reflectance of the aluminum sheet, the measured overall coupling efficiency by the reflector-collector system is about 7 percent.

6. Laser Output Dependence on Gas Pressure

The laser output for various gas fill pressures was measured in order to find the optimum pressure for the laser system. A germanium photodiode (JUDSON INFRARED Model J16LDO) which was calibrated by a He-Ne laser at 632.8 nm of known power, and the spectral sensitivity curve provided by the manufacturer, was used for the laser power measurements. The peak laser power as a function of gas pressure is plotted on figure 15. The optimum gas pressure for this laser system is near 30 torr.

7. Measurement of Photodissociation Rate

A typical laser output signal monitored in this experiment is shown in figure 16. For this run, the gas pressure was 30 torr and the applied electrical energy to the flashlamp was 135 J. As shown in figure 16, the laser oscillation starts around 14.5 μs after the onset of the flashlamp, or the threshold of laser action reaches after 14.5 μs of pumping of the $i-C_3F_7I$ gas. The threshold

photodissociation rate of the parent molecule ($i-C_3F_7I$) can be calculated by theoretical consideration using the absorption cross section of the parent molecule and spectral power distribution coupled into the laser tube. The threshold photodissociation rate can be expressed as

$$W = \int_{\lambda_o}\int^{t_{th}} \frac{\sigma_{ab}(\lambda) \cdot P(\lambda,t) \cdot \lambda \, d\lambda \, dt}{hc} \qquad (4)$$

where $\sigma_{ab}(\lambda)$ is the absorption cross section of the parent molecule, $P(\lambda,t)$ is the spectral input power per unit area per unit wavelength into the laser tube, h is Planck's constant, c is the velocity of light, and t_{th} is the start time of laser oscillation. The integration should be done in the absorption band of the parent molecule.

By using the previous experimental results of spectral power distribution of the flashlamp (fig. 7), and the pump light coupling efficiency by the reflector-collector system, the threshold photodissociation rate could be calculated from equation (4). In this calculation it was assumed that the laser tube was illuminated by the pump light isotropically, and that the spectral power output from the flashlamp was linearly increased in time until the light intensity reached its peak at 16 μs. And, also, it was assumed that when the parent molecule was excited by UV light in the absorption band, it dissociated only into perfluoroalkyl radical R and excited atomic iodine I*[12], i.e.,

$$[RI]^* \rightarrow I^* + R.$$
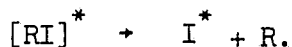
The calculated value of the threshold photodissociation rate W from equation (4) is 4.3×10^{-5}.

The pump energy used for the threshold photodissociation can be calculated by the relation

$$E_{th} = \int_\Omega \int_\lambda \int^{t_{th}} P_f(\lambda,t) \cdot \eta_{coup} \cdot d\lambda \, dt \, d\Omega \qquad (5)$$

where $P_f(\lambda t)$ is the spectral power output from the flashlamp, η_{coup} is the coupling efficiency of the reflector-collector system and Ω is the solide angle. The flashlamp used in this experiment is long so that it can be considered as a linear light source. Then, the integration of equation (5) with respect to solid angle is simply multiplication of 2π. And, the spectral range of the integration in equation (5) should be the same as the absorption band of the parent molecule i-C_3F_7I. With these considerations, the calculated pump energy for the threshold photodissociation from equation (5) was 0.045 J.

If we consider the parent molecule as an ideal gas, then the density in the laser tube is 9.6×10^1 molecules/cm^3 for 30 torr at room temperature (300 K). Multiplying the threshold photodissociation rate from equation (4), the density of the excited atomic iodine is calculated as

$$[I^*] = [RI] \times W = 9.6 \times 10^{17} \times 4.3 \times 10^{-5} = 4.1 \times 10^{13} \text{ atoms/cm}^3.$$

However, as mentioned in section 2, the excited atomic iodines are distributed in hyperfine levels of the excited state according to the degeneracy of each level so that the population density in F = 3 sublevel of the excited atomic iodine is $[I^*] \times 7/12 = 2.4 \times 10^{13}$ atoms/cm^3 (see fig. 2). And, the laser oscillation starts by the transition from F = 3 of the excited state to F= 4 of the ground state of the atomic iodine. Also at the beginning of the laser oscillation there is no population in the ground state. So the threshold inversion density of this laser system is 2.4×10^{13} atoms/cm^3.

The threshold inversion density can also be calculated by using the laser threshold condition. The laser threshold condition is given as

$$R_1 R_2 \exp (2\ell\, \sigma_{st}\, \Delta N_{th}) = 1 \tag{6}$$

where R_1 and R_2 are the reflectances of laser cavity mirrors, ℓ is the pumped length of laser tube, σ_{st} is the stimulated emission cross section of the laser

transition and ΔN_{th} is the population inversion density at the threshold. If the stimulated emission cross section σ_{th} is known, then the threshold inversion density ΔN_{th} can be calculated from equation (6) substituting the measured reflectances of the cavity mirrors ($R_1 = 0.998$, $R_2 = 0.98$) and the pumped length of the laser tube ($\ell = 116.5$ cm). However, the experimentally measured stimulated emission cross section of the transition from F = 3 of the excited state to F = 4 of the ground state of atomic iodine scatters over a rather wide range according to the researchers [20,21, 22]. If the result in reference 21 is adopted, then the stimulated emission cross section of the transition is 3.0×10^{-18} cm^2 at the i-C$_3$F$_7$I pressure of 30 torr. The calculated threshold inversion density from equation (6), with measured reflectances of the cavity mirrors, the pumped length of the laser tube, and the stimulated emission cross section, is $\Delta N_{th} = 3.2 \times 10^{13}$ atoms/cm^3, which is in good agreement with the result of the calculation by the photodissociation rate.

The maximum photodissociation rate is also estimated by using the laser threshold measurement with additional losses inserted in the laser cavity. The laser threshold condition for the cavity with a loss can be written as

$$R_1 R_2 \; L^2 \exp(2\ell \; \sigma_{st} \; \Delta N) = 1 \qquad (7)$$

where R_1 and R_2 are the reflectances of cavity mirrors, L is the loss factor for a single pass, ℓ is the gain length in the laser cavity, σ_{st} is the stimulated emission cross section of the laser transition, and ΔN is the population inversion density. A full reflector ($R_1 = 0.998$) and an output coupler ($R_2 = 0.85$) were used for laser cavity mirrors, the laser action was observed when the electrical energy ol 135 J was applied to the flashlamp (charging voltage of the storage capacitor, 10 KV) at the i-C$_3$F$_7$I gas pressure of 30 torr without any

loss inside the laser cavity. From this fact, the population inversion density calculated from equation (7) is

$$\Delta N > 2.4 \times 10^{14} \text{ atoms/cm}^3.$$

When the same full reflector and a different output coupler with reflectance $R_2 = 0.98$ were used for laser cavity mirrors, and a slide glass (Corning 2947) with transmittance 0.91 at 1.32 μm was inserted inside the laser cavity as a loss factor, the laser action was not observed. So, the population density calculated from the equation is

$$\Delta N < 3.0 \times 10^{14} \text{ atoms/cm}^3.$$

From the above two results, it can be concluded that the maximum population density in the F = 3 level of the excited state of the atomic iodine is

$$\Delta N = 2.7 \times 10^{14} \text{ atoms/cm}^3.$$

when the laser tube was pumped with electrical energy 134 J. The total photodissociation rate can be estimated from the above result as

$$\frac{2.7 \times 10^{14} \text{ atoms/cm}^3 \times (12/7)}{9.6 \times 10^{17} \text{ molecules/cm}^3}$$

where the factor 12/7 is included because the laser action is initiated only by the transition from F = 3 of excited state to F = 4 of ground state of the atomic iodine. So the total photodissociation is about 10 times larger than the threshold photodissociation when the present laser system is pumped by an electrical energy of 135 J.

When this laser tube is used for an amplifier tube, the energy stored in the tube can be estimated as

$$E_{st} = \Delta N \cdot h\nu_L \cdot V \tag{8}$$

where E_{st} is the stored energy inside the laser tube, ΔN is the total population density in the excited state of the atomic iodine (F = 3 and F = 2 of $^2P_{1/2}$), h is Planck's constant, ν_L is the laser frequency, and V is the volume of gain medium. The total population density in the excited state is calculated as

$$(2.7 \times 10^{14} \text{ atoms/cm}^3) \times (12/7) = 4.6 \times 10^{14} \text{ atoms/cm}^3$$

when the laser tube is filled with i-C_3F_7I gas at the pressure of 30 torr and is pumped with electrical energy of 135 J. The stored energy estimated from equation (8) for the present laser tube is 8.3 mJ in the wavelength of 1.32 μm.

8. Conclusion

In this experiment, an iodine laser system was developed to evaluate the concept of a direct solar-pumped laser amplifier. To simulate the solar radiation in space with a pulsed flashlamp, a parabolic cylindrical reflector-collector system was developed such that the reflector made the radiation from the flashlamp parallel and the collector concentrated the radiation into the laser tube. To compare the radiation from the flashlamp with the solar radiation in space, the spectral power output from the flashlamp was measured in the range of UV and visible of the spectrum. It was found that the spectral power distribution in the absorption band of the i-C_3F_7I molecule (250 nm ~ 300nm) from the flashlamp was nearly the same as that of the 6,000 K blackbody radiator when the flashlamp energized with electrical energy of 135 J.

The coupling efficiency of the pump light by the reflector-collector system was measured. The result showed that the overall coupling efficiency by the reflector-collector system was 7 percent in the absorption band of the i-C_3F_7I molecule.

The optimized i-C_3F_7I gas pressure inside the laser tube, the laser

output was measured as a function of the gas pressure   The optimum pressure for the present laser system was 30 torr when the laser tube was pumped with electrical energy 135 J.

The threshold photodissociation rate of the $i-C_3F_7I$ gas was measured by using the measured result of the spectral power distribution of the flashlamp and the measured optical coupling efficiency by the reflector-collector system. The result showed that the threshold population density in the excited state of atomic iodine was 2.4×10^{13}. This result was compared with the calculation from the laser threshold condition and showed a good agreement. At the same time the pump energy used for the threshold photodissociation was calculated to be 45 mJ in the absorption band of the $i-C_3F_7I$ molecule.

Also, the total population inversion was measured from the laser threshold condition by changing the output coupler mirror or inserting a loss in the laser cavity. The total population density in the excited state of atomic iodine was 4.6×10^{14} atoms/cm^3 when the laser tube was filled with $i-C_3F_7I$ gas at 30 torr pressure and was pumped with electrical energy of 135 J. And, the stored energy was calculated from the measured total population and was found to be 8.3 mJ in case the laser tube was used for laser amplifier.

REFERENCES

1. Lee Ja H.; and Weaver, W. R: A Solar Simulator-Pumped Atomic Iodine Laser. Appl. Phys. Lett. $\underline{39}$, 137, 1981.

2. Zapata, L. E.; De Young, R. J.: Flashlamp-Pumped Iodine Monobromide Laser Characteristics. J. appl. Phys. $\underline{54}$, 1686, 1983.

3. Hongyo, M.; Sasaki, T.; Nagamo, Y.; Ueda, K.; and Yamanaka, C.: High-Power $Nd^{+3}POCl_3$ Liquid Laser System. IEEE J. Quant. Electron. $\underline{QE-8}$, 192, 1972.

4. Yesil, O.; and Christiansen, W. H.: Optically Pumped Carbon Dioxide Laser Mixtures. J. Energy $\underline{3}$, 315, 1979.

5. Kasper, J. V. V.; and Pimentel, G. C.: Atomic Iodine Photodissociation Laser. Appl. Phys. Lett. $\underline{5}$, 231, 1964.

6. Brederlow, G.; Brodmann, R.; Edimann, K.;Nippus, M.; Petsch, R.: Witkowski, S.: Volk, R.; and Witte, J.: Performance of the Asterix III High Power Iodine Laser. IEEE J. Quant. Electron. $\underline{QE-16}$, 122,

7. Zuev, V. S.; Katulin, V. A.; Nosach, V. Yu; and Nosach, O. Yu: Investigation of the Luminescence Spectrum of Atomic Iodine ($^2P_{1/2}$ – $^2P_{3/2}$ Laser Transition). Sov. Phys. JETP 35, 870, 1972.

8. Garstang, R. H.: Transition Probabilities of Forbidden Lines. J. Research of Nat. Bur. of Std.-A, Physics and Chemistry $\underline{68A}$, 61, 1964.

9. Derwent, R. G.; and Thrush, B. A.: The Radiative Lifetime of the Metastable Iodine Atom $I(5^2P_{1/2})$. Chem. Phys. Lett. $\underline{9}$, 591, 1971.

10. Baker, H. J.; and King, T. A.: Repetitively Pulse Iodine Laser with Thermal Gas Flow Cycle. J. Phys. D.: Appl. Phys. $\underline{14}$, 1367, 1981.

11. Ershov, L. S.; Zalesskii, Y. Yu; and Sokolov, V. N.: Laser Photolysis of Perfluoroalkyl Iodide. Sov. J. Quant. Electron. $\underline{8}$, 494, 1978.

12. Pravilov, A. M.: Spectroscopy and Primary Processes in the Photolysis of Iodides for Iodine Photodissociation Lasers (Review). Sov. J. Quant. Electron. $\underline{11}$, 848, 1981.

13. Wilson, J. W.; and Lee, J. H.: Modeling of a Solar-Pumped Iodine Laser. Virginia J. of Science $\underline{31}$, 34, 1980.

14. Wilson, J. W.: Raju, S.; and Shiu, Y. J.: Solar-Simulator-Pumped Atomic Iodine Laser Kinetics. NASA TP-2182, 1983.

15. Zalesskii, V. Yu.: Iodine Laser Pumped by Solar Radiation. Sov. J. Quant. Electron. $\underline{13}$, 701, 1983.

16. Magdeburg, H.: Spektraler Emissionsgrad und Strahldichte des Niederstrom-Kohlebogens. Z. Naturforsch. $\underline{20a}$ 980, 1965.

17. Hattenberg, A. T.: Spectral Radiance of a Low Current Graphite Arc. Appl. Opt. $\underline{6}$, 95, 1967.

18. KODAK Plates and Films, Eastman Kodak Co., Scientific and Technical
     DATA P-9, Eastman Kodak, New York, 1967.

19. Weaver, W. R.: Unpublished data.

20. Palmer, ?. E.; and Gusinow, M. A.: Late-time Gain of the CF_3I Iodine
     Photodissociation Laser. J. Appl. Phys. 45, 2174, 1974.

21. Baker, H. J; and King, T. A.: Iodine Photodissociation Laser
     Oscillator Characteristics. J. Phys. D.: Appl. Phys. _8_, 609, 1975.

22. Babkin, V. I.; Kuznetsova, S. V.; and Maslov, A. I.: Simple Method
     for Determination of Stimulated Emission Cross Section of $^2P_{1/2}$
     $(F = 3) \rightarrow {}^2P_{3/2}$ $(F' = 4)$ Transition in Atomic Iodine. Sov. J.
     Quant. Electron. _8_, 285, 1978.

Fig.2. Atomic iodine level structure and relative fluorescence intensity.

Fig.1. Processes leading to iodine photodissociation laser.
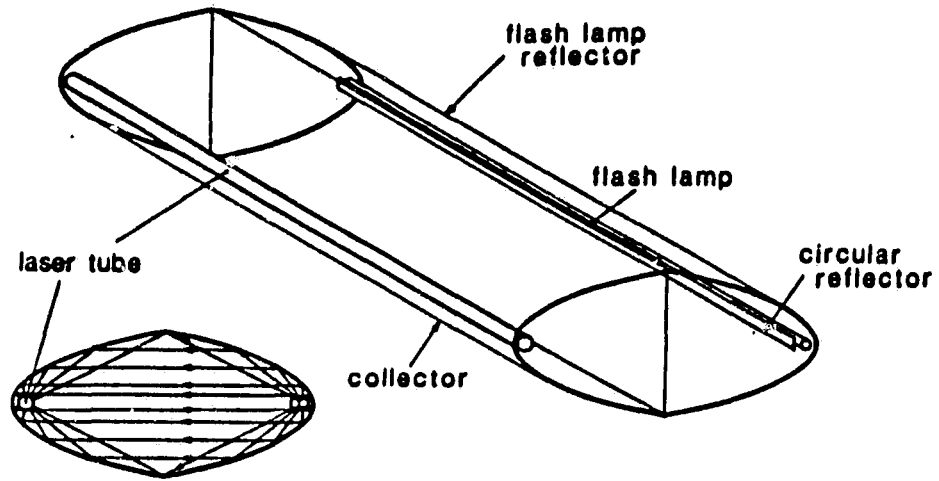
Fig.3. Laser system design.
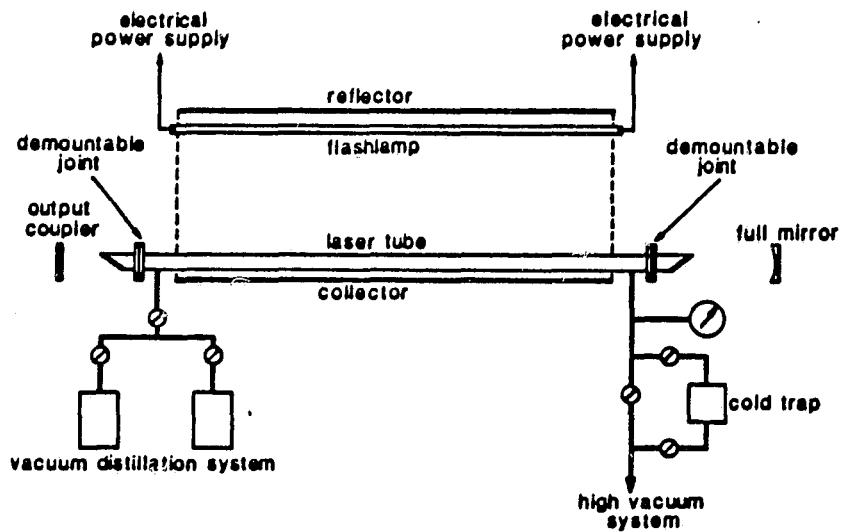
Fig.4. Gas handling system and optical cavity for iodine laser.
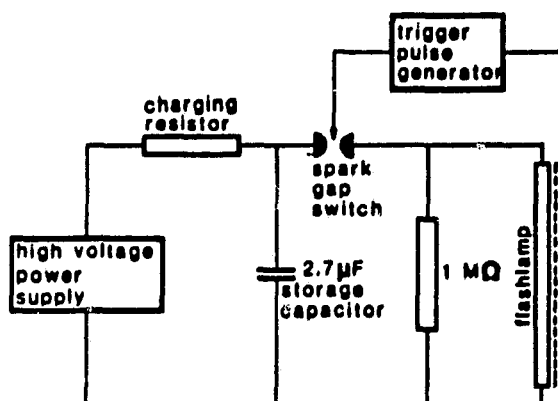
Fig.5. Electrical circuit for flashlamp.
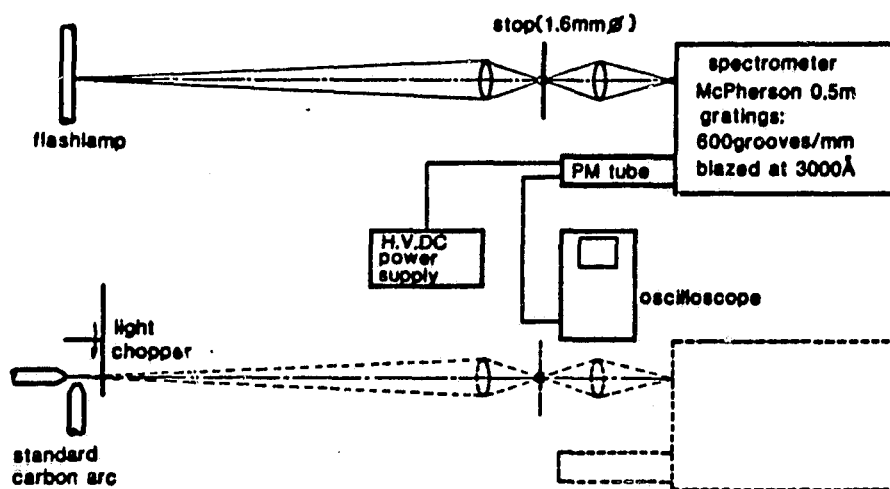
Fig.6. The experimental setup for the measurement of spectral output power from the flashlamp.

68
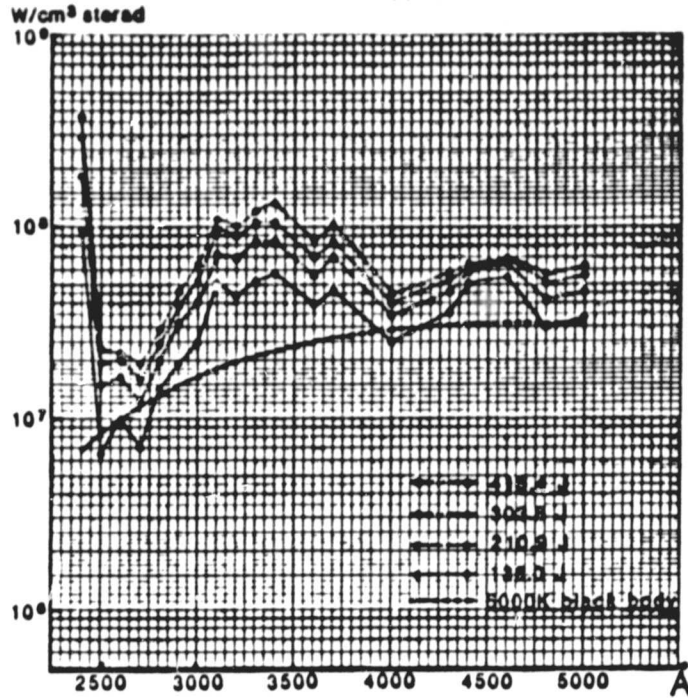
Fig.7. Spectral peak power output from the flashlamp
for various electrical energy.
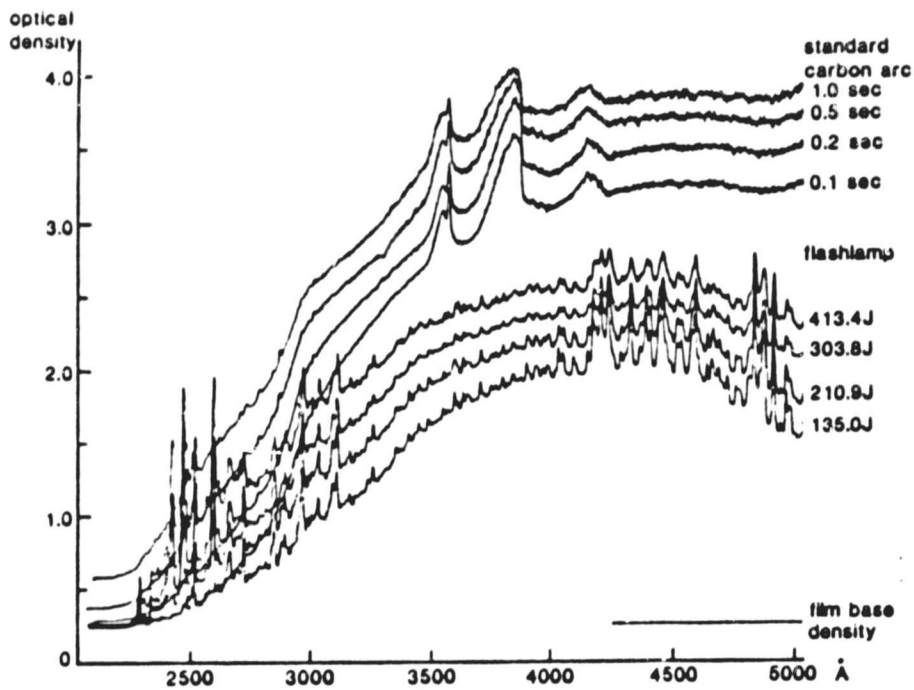
Fig.8. Densitometric traces for the standard carbon arc and the flashlamp.
The tri-X pan film was used.
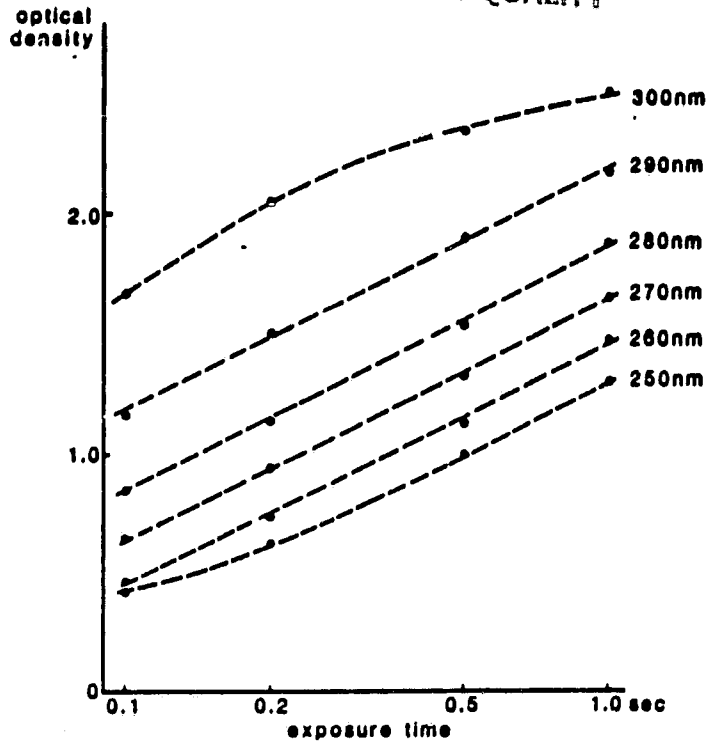
Fig.9.The measurement of the contrast index.
The measured C.I. was 1.0 at the wavelengths
260nm,270nm,280nm and 290nm.
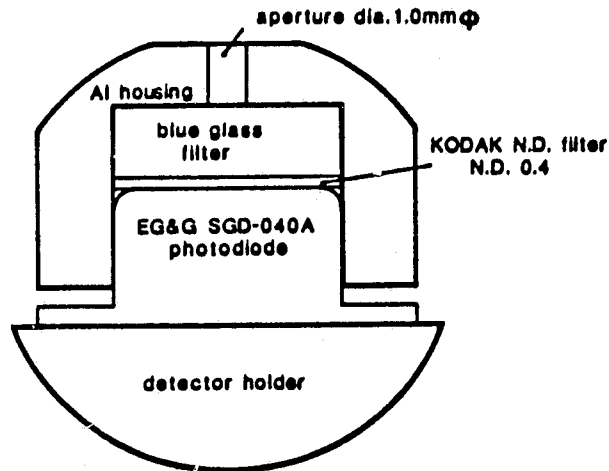
Fig.10. Modification of photodiode used in the experiment.

70
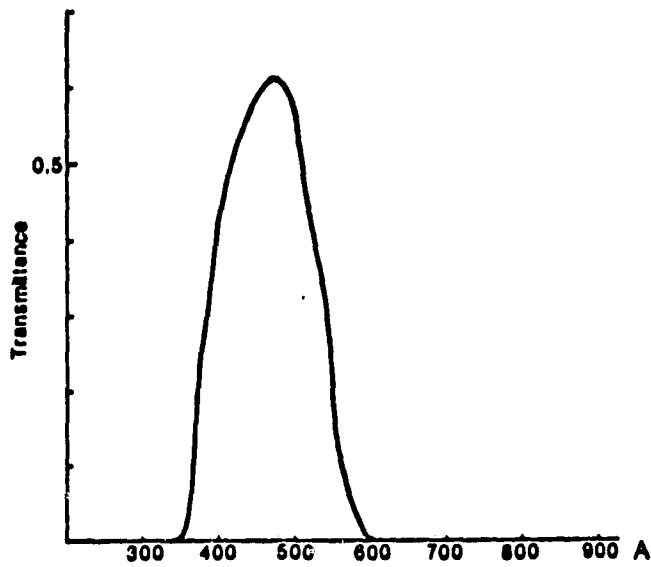
Fig. 11. Transmittance of blue glass filter.
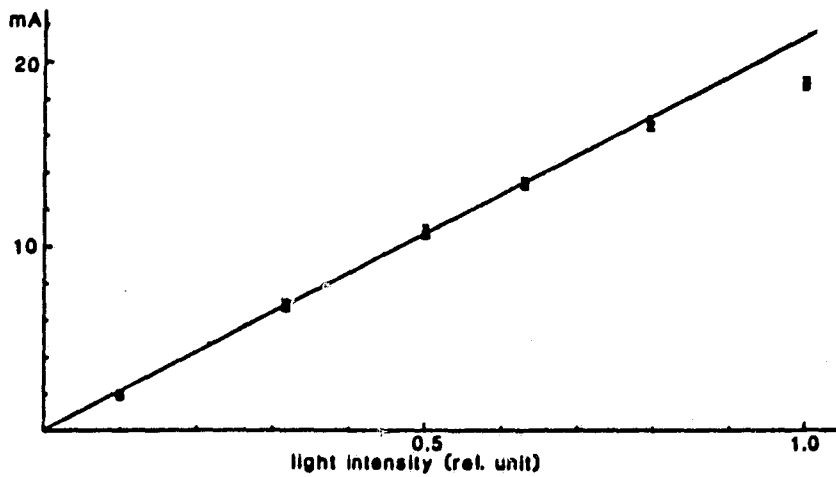
Fig. 12. Response of photodiode for different light intensity.

Negative bias:90V,load resistor:50Ω.
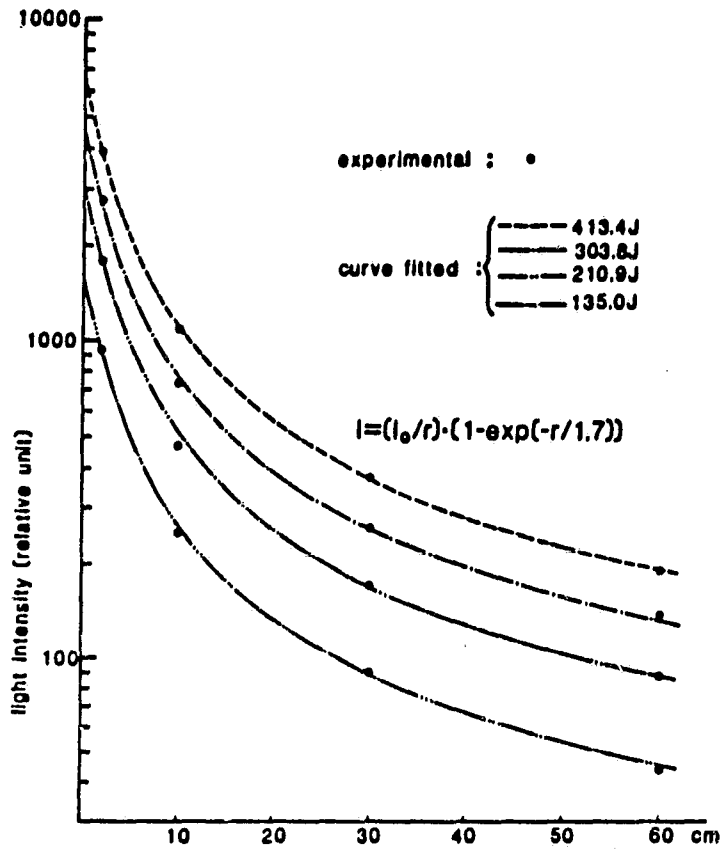
Fig. 13. Light intensity at different electrical energy
and at different distance from flashlamp.

72
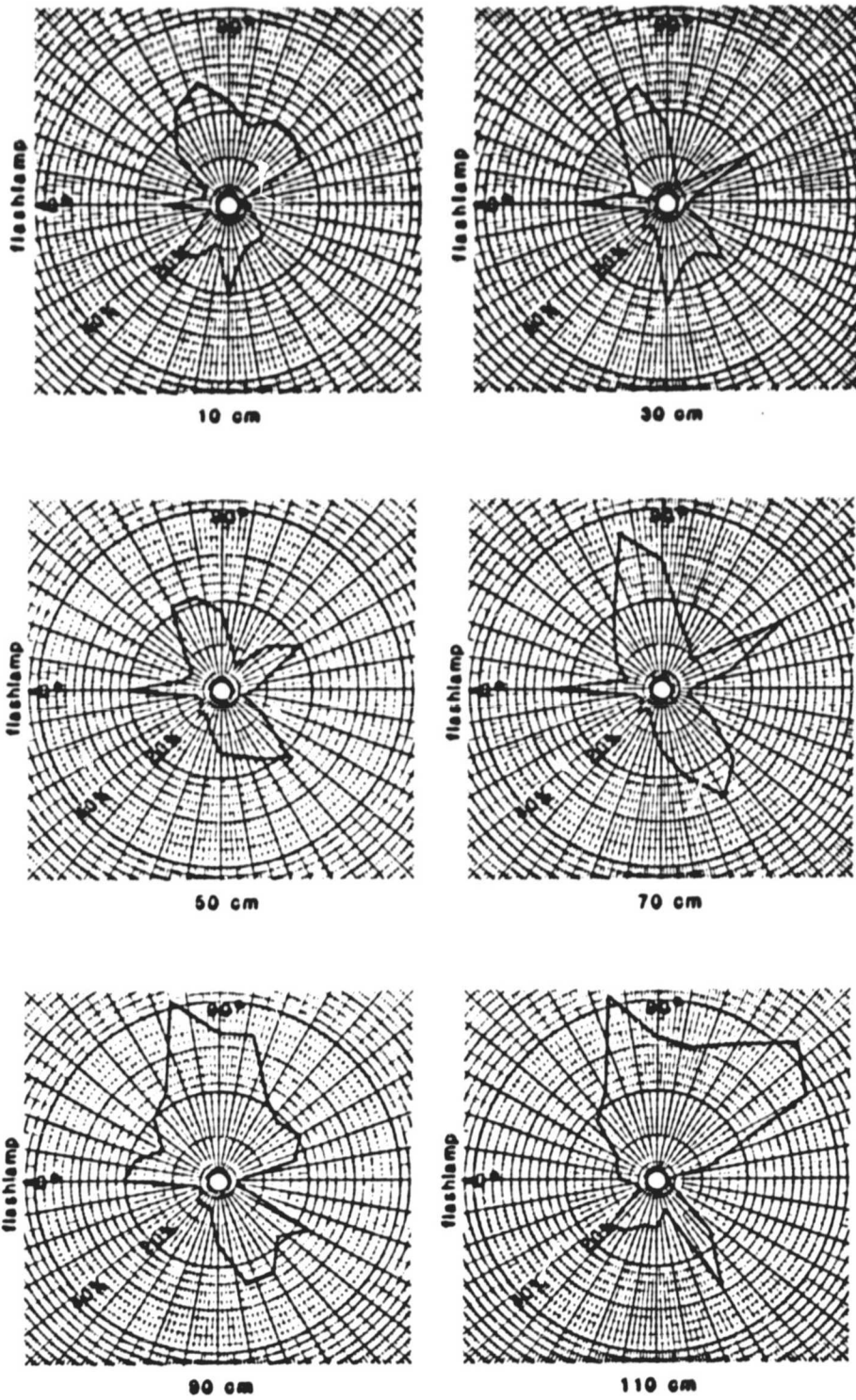
Fig. 14. Radial distribution of pumping light intensity at different positions along the laser tube axis. The distances are measured from one end of pumped laser tube.
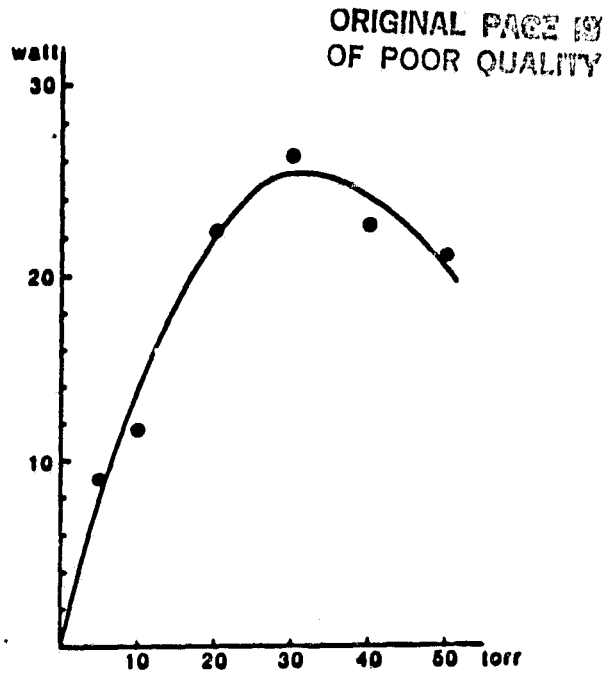
Fig.15. Peak laser output power dependence on
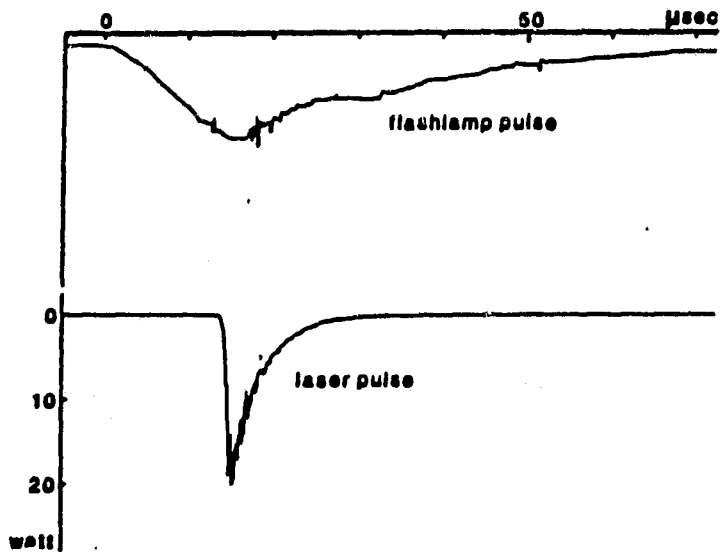**i-C_3F_7I gas fill pressure.**
Applied electrical energy: 135J.

Fig.16. A typical laser output pulse. Electrical energy: 135J.

Direct Solar-Pumped Lasers

Ja H. Lee,
Vanderbilt University, Nashville, TN .37235

Y. J. Shiu
Hampton Institute,,Hampton, VA 23668

and

NASA langley Research Center, Hampton, VA 23665

Abstract

The feasibility of direct solar pumping of high-power lasers is being investigated and one of the candidates, an iodine photodissociation laser at $\lambda = 1.315$ μm, was tested. Threshold inversion density, effect of elevated temperature (to 670K) on the laser output, and laser gain from a cavity filled with C_3F_7I vapor irradiated by a 32-kW solar simulator were measured. These results and the concentration of solar radiation required for the solar'pumped iodine laser will be disscussed.

APPENDIX II

ABSTRACT – NASA TECHNICAL REPORT 2182 SOLAR SIMULATOR-PUMPED ATOMIC IODINE
LASER KINETICS

John W. Wilson
NASA Langley Research Center
Hampton, VA 23665

S. Raju and Y. J. Shiu
Hampton Institute
Hampton, VA 23668

ABSTRACT

The literature contains broad ranges of disagreement in kinetic data for
the atomic iodine laser. A kinetic model of a solar-simulator-pumped iodine
laser is used to select those kinetic data consistent with recent laser experiments
at the Langley Research Center. Analysis of the solar-simulator-pumped laser
experiments resulted in the following estimates of rate coefficients: for alkyl
radical (n-C_3F_7) and atomic iodine (I) recombination, 4.3×10^{-11} $(1.9)^{\pm 1}$ cm^3/s;
for n-C_3F_7I stabilized atomic iodine recombination (I + I) 3.7×10^{-32} $(2.3)^{\pm 1}$
cm^6/s; and for molecular iodine (I_2) quenching 3.1×10^{-11} $(1.6)^{\pm 1}$ cm^3/s. These
rates are consistent with the recent measurements.